



South Texas Project Electric Generating Station P.O. Box 289 Wadsworth, Texas 77483

July 20, 2009  
U7-C-STP-NRC-090072

U. S. Nuclear Regulatory Commission  
Attention: Document Control Desk  
One White Flint North  
11555 Rockville Pike  
Rockville, MD 20852-2738

South Texas Project  
Units 3 and 4  
Docket Nos. 52-012 and 52-013  
Responses to Requests for Additional Information

Attached are responses to NRC staff questions included in Request for Additional Information (RAI) letters numbered 116, 117, and 127, related to Combined License Application (COLA) Part 2, Tier 2, Section 2.5S.4, Stability of Subsurface Materials and Foundations, Section 2.5S.2, Vibratory Ground Motion, and Section 2.5S.1, Basic Geologic and Seismic Information, respectively. This submittal forms a complete response to RAI letters numbered 116 and 127.

Attachments 1 through 8 provide responses to the following RAI questions:

02.05.04-22	02.05.02-19	02.05.01-18
02.05.04-23	02.05.02-20	02.05.01-19
		02.05.01-20
		02.05.01-21

When a change to the COLA is indicated, the change will be incorporated into the next routine revision of the COLA following NRC acceptance of the RAI response.

There is one commitment in this letter and it is summarized in Attachment 9.

If you have any questions regarding these responses, please contact me at (361) 972-7206, or Bill Mookhoek at (361) 972-7274.

DO91  
MRO

I declare under penalty of perjury that the foregoing is true and correct.

Executed on 7/20/2009



Mark McBurnett  
Vice President, Oversight and Regulatory Affairs  
South Texas Project Units 3 & 4

rhb

Attachments:

1. Question 02.05.04-22
2. Question 02.05.04-23
3. Question 02.05.02-19
4. Question 02.05.02-20
5. Question 02.05.01-18
6. Question 02.05.01-19
7. Question 02.05.01-20
8. Question 02.05.01-21
9. Commitment Summary

cc: w/o attachments and enclosure except\*  
(paper copy)

Director, Office of New Reactors  
U. S. Nuclear Regulatory Commission  
One White Flint North  
11555 Rockville Pike  
Rockville, MD 20852-2738

Regional Administrator, Region IV  
U. S. Nuclear Regulatory Commission  
611 Ryan Plaza Drive, Suite 400  
Arlington, Texas 76011-8064

Kathy C. Perkins, RN, MBA  
Assistant Commissioner  
Texas Department of Health Services  
Division for Regulatory Services  
P. O. Box 149347  
Austin, Texas 78714-9347

Alice Hamilton Rogers, P.E.  
Inspections Unit Manager  
Texas Department of Health Services  
P. O. Box 149347  
Austin, Texas 78714-9347

C. M. Canady  
City of Austin  
Electric Utility Department  
721 Barton Springs Road  
Austin, TX 78704

\*Steven P. Frantz, Esquire  
A. H. Gutterman, Esquire  
Morgan, Lewis & Bockius LLP  
1111 Pennsylvania Ave. NW  
Washington D.C. 20004

\*George F. Wunder  
\*Tekia Govan  
Two White Flint North  
11545 Rockville Pike  
Rockville, MD 20852

(electronic copy)

\*George Wunder  
\*Tekia Govan  
Loren R. Plisco  
U. S. Nuclear Regulatory Commission

Steve Winn  
Eddy Daniels  
Joseph Kiwak  
Nuclear Innovation North America

Jon C. Wood, Esquire  
Cox Smith Matthews

J. J. Nesrsta  
R. K. Temple  
Kevin Polló  
L. D. Blaylock  
CPS Energy

**RAI 02.05.04-22****Question**

There is very little information in the FSAR regarding the presence of fissures and slickensides in the Beaumont clay, whereas FSAR reference 2.5S.4-14A by Mahar and O'Neil address the difficulties of measuring soil properties of stiff fissured clays both in the lab and insitu. Since the referenced work is based on Beaumont clay, and is the basis for some of your assumptions regarding engineering properties of the site soils, the staff believes it would be helpful that you address more fully the nature and distribution of fissures and slickensides with respect to that presented in reference 2.5S.4-14A.

Please provide a thorough discussion regarding the dessication features you encountered in the Beaumont clay. Please discuss how the dessication features compare to that presented in the reference 2.5S.4-14A. Please indicate how the various laboratory and insitu test results are conservative in the evaluation of the engineering properties used for bearing capacity, slope stability and settlement analyses.

**Response**

Features indicative of desiccation observed within the soil samples from the Beaumont formation obtained during project geotechnical explorations were slickensides, fissures, and calcareous deposits. These features are consistent with the features described in Reference 2.5S.4-14A. These features can create inherent local planes of weakness within the soil samples. During typical strength and compressibility laboratory testing, failure often occurs along these planes of weakness, which can contribute to failure at a strength lower than would occur in their in situ condition. Reference 2.5S.4-14A also notes a "pointwise and directional variability in shear strength" from laboratory tests. This is partially a result of the inability in laboratory tests on small samples to replicate the condition of a larger in situ mass of soil with its local slickensides. The sampling process also probably resulted in sample disturbance to varying degrees due to the release of lateral and vertical confinement and overburden pressures of these soils in situ particularly at deeper depths. These conditions are noted in the response to RAI 02.05.04-13, submitted on February 23, 2009 (proposed markup to FSAR 2.5S.4.2.1.4), as possible reasons for low strength to vertical effective stress ratios and exclusion of some of the laboratory strength tests when selecting strength parameters.

Selection of engineering properties for use in bearing capacity and settlement analysis was based on data from several different field techniques including standard penetration tests (SPT), cone penetration test (CPT), geophysical, strength and compressibility laboratory testing including unconfined compression, unconsolidation-undrained triaxial, consolidation-undrained triaxial, and consolidation testing. Reference 2.5S.4-14A supports this engineering property selection with an indication that "nonconventional" laboratory and in situ tests, or both, appear desirable to provide further insight into the in situ behavior of the soils. Although it is possible that the strength results of laboratory tests performed on individual samples are not indicative of actual in-situ strengths of the soil mass on a scale appropriate for bearing capacity analyses, the

laboratory tests in general would have produced lower strength parameters or conservative properties for use in bearing capacity (and settlement) analysis. However, laboratory test results were not the sole basis for selection of the parameters. The results of the laboratory tests were compared to the results of the field test soils under in situ conditions and typical and conservative values were selected.

FSAR Section 2.5S.4.5 addresses temporary deep excavations. Note a response to Question 632/RAI 02.05.04-2 regarding temporary excavation slope was previously submitted as part of Response to Requests for Additional Information, ABR-AE-08000074, on October 1, 2008. Section 2.5S.5 of the FSAR contains information about stability of permanent constructed and natural slopes. Please note that there are no nuclear safety related slopes constructed as part of the COL application for Units 3 & 4. Thus, no discussion regarding impact of parameters to slope stability is included in this response.

No COLA revision is required as a result of this RAI response.

**RAI 02.05.04-23****Question:**

The FSAR supplemental exploration data contains CPT soundings that show high pore water pressure response in a zone of silt (based on soil behavior type) in the depth range of 48 feet to 60 feet and 80 feet to 100 feet (reference CPT soundings C-304 and C-305s, for example). Similar high pore water pressure response is observed in other soundings across the site occurring at various depths, but typically below 48 feet. This appears to correspond to layers D and F in FSAR Section 2.5.4.2. The staff understand that high pore water pressure response is normally associated with contractive behavior, and more near normally consolidated soils. OCR average values determined from site-wide CPT soundings for the depths under consideration are shown to range from 4.2 to 1.7, as shown on FSAR Figure 2.5S.4-33. The range of individual OCR predictions from CPT measurement are very widely spread between approximate depths of 40 and 65 feet in this figure.

Please discuss how you interpret the high pore water pressure response measured in the overconsolidated clay soils. Since your strength determinations for layers D and F use OCR relationships to evaluate insitu shear strength, is there concern that the high pore water pressure response observed in the CPT data may indicate lower OCR values and consequently lower undrained shear strength? Please justify your strength parameters for layers D and F in light of the CPT pore water pressure response.

**Response:**

Responses measured behind the cone tip in heavily over-consolidated soils ( $OCR > 10$ ) are typically expected to be zero or negative. The measured pore pressure responses in Strata A and B are indicative of heavily over-consolidated materials.

However, pore pressure responses only provide an indication if the materials are not heavily over-consolidated. The pore pressure response in the D and F Layers as compared to similar published responses measured in the Beaumont (References 2.5S.4-10A and 2.5S.4-14A) exhibits both normally consolidated and lightly over-consolidated qualities.

Published CPT correlations for OCR were developed from correlations with laboratory consolidation tests. To this extent, oedometer tests are the accepted method for estimating soil stress history. Thus, laboratory consolidation test results from the D and F Layers are the governing data set. The CPT correlations provide primarily a means to confirm and augment the laboratory consolidation results.

The CPT correlation for undrained shear strength used a site-specific "cone factor" developed using the laboratory-measured values of shear strength. The cone factor thus developed was at the upper end of the range of published values. The tip resistances, a high cone factor developed using laboratory strength data, and total overburden stresses constitute the input for estimating undrained shear strength for the CPT. Additionally, standard penetration tests and a conservative

published correlation were used to assist in selection of the undrained shear strength values. Therefore, the pore pressure responses observed in the CPT data from the D and F Layers are not a concern.

No COLA revision is required as a result of this RAI response.

**RAI 02.05.02-19****Question:**

In your FSAR Com 2.5S-1, you summarized the process to incorporate 16 RC/TS testing results for soil dynamic properties and presented two sample plots to illustrate the sample testing results and the comparison between these samples and EPRI generic curves or Vucetic and Dobry curves. You also described that you modified the onsite generic deep shear wave velocity profile using three oil well geophysical data. Because Sections 2.5S.4.7.3, "Static and Dynamic Laboratory Testing" and 2.5S.2.5, "Seismic Wave Transmission Characteristic of the Site" were significantly affected by these updates, please provide complete contents for those sections, including all supporting figures, for example, sample's modulus reduction and damping curves for foundation supporting soil layers and maximum strain curves. In addition, please include P and S wave profiles from those oil wells and the final shear wave velocity profile used in site response analysis.

**Response:**

STP COLA Part 2, Tier 2, Subsection 2.5S.2.5, "Seismic Wave Transmission Characteristic of the Site," and Subsection 2.5S.4.7, "Response of Soil and Rock to Dynamic Loading," are presented below. Revised Tables and Figures supporting these sections will be provided in a supplement to this RAI by August 9, 2009. Subsection 2.5S.4.7.2.2.2, "Bedrock Shear Wave Velocity Profile," which is included below, addresses the final shear wave velocity profile used in site response analysis. All of the changes shown below, including supporting Tables and Figures, will be included in the next scheduled update of the COLA.

STP COLA Part 2, Tier 2, Subsection 2.5S.2.5, "Seismic Wave Transmission Characteristic of the Site," will be revised as shown below:

**2.5S.2.5 Seismic Wave Transmission Characteristics of the Site**

The UHRS described in the previous section are defined on hard rock characterized with shear wave velocity  $V_s = 9200$  fps, which is located at more than 30,000 feet (9144 m) below the ground surface. This section describes the development of the site amplification factors that result from the transmission of the seismic waves through the thick soil column. The effect is modeled by a truncated soil column, extending from the ground surface to a depth of about ~~30,000~~ 8100 feet (~~9144~~ 2469 meters), and an adjustment to the soil damping within the truncated soil column to represent the anelastic attenuation of ground motion by the entire soil column (the "kappa" value).

The development of the site amplification factors is performed in the following steps:

- (1) Develop a model of the base case soil column using site-specific geotechnical and geophysical data to a depth of about 600 feet (182 meters), augmented to a depth of about ~~3000~~ 8100 feet (~~914~~ 2469 meters) with deep velocity profiles taken obtained from EPRI (Reference 2.5S-2-12) available deep sonic log data. The model for the upper 600 feet (182 meters) is based on mean shear wave velocities measured at the site and shear modulus and damping strain dependencies taken

from selected generic curves (Reference 2.5S.2.12) to match the Resonant Shear Column Torsional (RCTS) testing results (see Subsection 2.5S.4.7). The deeper soil layers are assumed to behave linearly. This model provides the base case representation of the dynamic properties of STP 3 & 4 site subsurface.

- (2) Confirm, through sensitivity analyses, that this model adequately captures the frequency-dependent response of the deep soil column over all frequencies of interest.
- (3) Calculate strain-independent (linear-elastic) material damping values for the deep soil strata (182 to 914 meters/600 to 8100 ft), which experience small levels of strain during the earthquake to ensure that the truncated site model accurately accounts for the dissipation of energy in the deep soil site. This is done by constraining the damping within these deeper strata to replicate an estimate of the total kappa for the site.
- (4) Generate a set of 60 artificial "randomized" soil profiles by using the base soil column and developing a probabilistic model that describes the uncertainties in the above soil properties, location of layer and hard rock boundaries, correlation between the velocities in adjacent layers and the overall dissipation of energy in the site. Use the  $10^{-4}$  and  $10^{-5}$  annual-frequency-of-exceedance smooth LF and HF hard rock spectra of Subsection 2.5S.2.4 for input into the base of the randomized soil columns, calculate dynamic response of the site for each of the 60 artificial profiles by using an equivalent-linear site-response formulation together with Random Vibration Theory (RVT), and calculate the mean and standard deviation of site response. Time histories for the site response analysis are not required for the frequency-domain RVT approach to site response analysis. This step is repeated for each of the four input motions ( $10^{-4}$  and  $10^{-5}$  annual frequencies, HF and LF smooth spectra).

These steps are described in detail in the following subsections. The resulting site-specific amplification factors ARS are used with the hard rock spectra of Subsection 2.5S.2.4 to develop GMRS in Subsection 2.5S.2.6

#### **2.5S.2.5.1 Base Case Soil Column and Uncertainties**

Development of a base case soil column is described in detail in Subsection 2.5S.4. Summaries of the low strain shear wave velocity, material damping, and strain-dependent properties of the base case soil strata are provided below in this section. These parameters serve as input for the site response analyses.

The geology at the STP 3 & 4 site consists of deep marine and fluvial deposits overlying bedrock. The upper approximately 600 feet (182 m) of the site soils were investigated using test borings, Cone Penetration Testing (CPT), test pits, and geophysical methods. Based on the results from these tests, soils in the upper layers of the site can generally be divided into the following geotechnical strata:

- Stratum A: Clay (CH), medium stiff to very stiff

- Stratum B: loose to dense Silty Sand (SM) and sandy silt (ML), or medium stiff to very stiff clay
- Stratum C: Silty Sand (SM), dense to very dense
- Stratum D: Silty Clay (CH), very stiff to hard
- Stratum E: Slightly Silty Fine Sand (SP-SM), dense to very dense
- Stratum F: Silty Clay (CH/CL), very stiff to hard
- Stratum H: Silty Sand (SM), very dense
- Stratum J: Silty Clay (CL/CH) with Interbedded Silt, Silty Sand, Clayey Sand, or Sand, hard
- Stratum K: Sandy Clay, with Interbedded Silt or Silty Sand, stiff to hard
- Stratum L: Silty Clay (CL/CH), very stiff to hard
- Stratum M: Silty Sand (SM), dense to very dense
- Stratum N: Silty Clay (CH) with Interbedded Sand or Silty sand, very stiff to hard

The Primary-Secondary (P-S) suspension measurements and CPT results provided shear and compression wave velocities of the soil at 1.6 feet (0.5 m) intervals. These data were used to develop mean shear wave profile for the upper 600 feet (182 m) of soil. Unit weights for the upper 600 feet (182 m) soil are in the range of 120 pounds per cubic foot (pcf) to 128 pcf.

Generic EPRI curves (Reference 2.5S.2-12) were adopted to describe the strain dependencies of shear modulus and damping for the nonlinear degradation soil shear modulus and damping curves based on RCTS test results are described in Section 2.5S.4.7.3, and are used for the upper 600 feet (182 m) of soils. For cohesionless soils, eight sets of shear modulus and damping degradation curves were interpolated from the generic EPRI curves based upon approximate mid-thickness depth of soil strata or sub-strata, as shown in Figures 2.5S.4-57 and 2.5S.4-59. Five sets of curves were developed for the cohesive soils by interpolating from the generic EPRI curves based on the clay Plasticity Index (PI), shown in Figures 2.5S.4-58 and 2.5S.4-60. An alternative set of the strain dependent properties was developed for the cohesionless soils by using Peninsular curves from a Brookhaven National Laboratory report (Reference 2.5S.2-47) where two sets of stiffness and damping curves were used for the cohesionless soils at depths above and below 50 feet (15 m) depth. Numerical values of the recommended curves are provided in Table 2.5S.4-34b (degradation soil shear modulus) and Table 2.5S.4-34c (damping ratio).

Information on subsurface conditions for depths below approximately 600 feet (182 m) and extending to the maximum drilling depth of 2620 feet (798 m) was assembled from available sonic log data and used to develop the shear-wave velocity profile as well as other properties such as Poisson's ratio, refer to Section 2.5S.4 the Updated Final Safety Analysis Report (UFSAR) (Reference 2.5S.2-36) for the existing STP 1 & 2 that are located approximately 1500 feet (500 m) to 2500 feet (833 m) from STP 3 & 4 site. At depths below

600 feet (182 m), the soil profile consists of alternating layers of very stiff to hard clay (with some claystone and siltstone) and very dense, fine to silty fine sand. The claystone and siltstone occur at depths greater than approximately 880 feet (268 m) and frequency of occurrence increases with depth. Three cases of shear wave velocity profiles with different probability weights were developed for the deep soil strata based on EPRI (Reference 2.5S.2-48). Linear elastic properties are assigned to the soil at depths below 600 feet (182 m) by assuming that the strains in these deep soil layers remain small during the earthquakes. Unit weight of the deep soils (below approximately 600 feet, 182 meters) range from 129 pcf to 135-140 pcf. A value of 140-170 pcf was assigned for the bedrock unit weight.

Damping values were developed for the linear deep soil layers to maintain the total kappa for the site as described below.

Low-strain kappa (k) value, a near surface damping parameter for modeling site-dependent effects, is used as a measure of the total dissipation of energy of the site during the small strain events. The site kappa (k) value is directly related to damping of the soil layers and scattering of the waves at layer interface boundaries. The kappa associated for soil layer damping is additive for all layers. The following expression shows the relationship between kappa (ki) and the damping coefficient, (zi) of the soil layer (i):

$$\kappa_i = \frac{2H_i \xi_i}{V_{s_i}} \quad \text{Equation 2.5S.2-6}$$

where: Hi is the thickness and Vsi is the shear wave velocity of the soil layer (i). Total kappa (k) value of the site associated with material damping equals the sum of the ki values of all soil layers included in the model:

$$\kappa = \sum_i \kappa_i \quad \text{Equation 2.5S.2-7}$$

The value of total kappa (k) is directly evaluated from recordings of earthquakes. One of the nearest and most applicable measures of total kappa is a value of 0.058 sec based on inversions of regional earthquakes located and recorded within the deeper portions of the Mississippi Embayment in the area just south of Saint Louis, Missouri and Memphis, Tennessee (Reference 2.5S.2-49). For various other study areas in the Mississippi Embayment also lacking in direct measurements of total (k), a more conservative value (i.e., corresponding to lower damping) of 0.046 sec has been used (Reference 2.5S.2-48).

A kappa (k) value of 0.006 sec is assumed to apply to the central and eastern United States crystalline basement and below (Reference 2.5S.2-12), leaving a total soil kappa (k) value of 0.040 sec for the damping of the full depth of the Mississippi Embayment soils. EPRI (Reference 2.5S.2-12) presents a standard deviation of 0.4 natural log units to be appropriate for sites in the eastern United States. This is consistent with Reference 2.5S.2-48 in considering  $\pm 50\%$  variation about the base case value of kappa (k) for Mississippi embayment sites. Therefore, a base case kappa (k) value of 0.040 sec is used for STP 3 & 4 site model with a standard deviation of 0.4 natural log units.

The following procedure is used to assign the damping to the models of the soil at depths below 600 feet (182 m) in order to match the assigned kappa ( $\kappa$ ) value:

- (1) From Equations 2.5S.2-6 and 2.5S.2-7, kappa ( $\kappa$ ) associated with material damping is calculated for the top 600 feet (182 m) of soil strata by using small strain damping for each soil layer.
- (2) The kappa ( $\kappa$ ) value of the top 600 feet (182 m) of soil is deducted from the total kappa ( $\kappa$ ) value, and a constant damping value is assigned to deep soil layers. In this calculation the kappa associated with scattering of the waves in the randomized profiles is computed to ensure the kappa associated with both soil layer damping with scattering of the waves in the layered profiles maintains the total kappa adopted for the deep soil profile at the site.
- (3) The damping of each deep soil layer is randomized with consideration given to the mean and variation of the total kappa.

The input motion for soil amplification analysis was specified at the bottom of the soil profile, below which the halfspace was modeled with shear wave velocity of 9200 fps and a damping ratio of 0.2%.

Selection of base soil profile for the STP 3 & 4 site considered the effects of variation of several different input parameters. Analysis showed that the differences in calculated site responses obtained from three different EPRI (Reference 2.5S.2-48) deep soil models were not significant. Nevertheless, a weighted average of the three profiles was selected for this part of the base case model. Another sensitivity analysis showed that the difference between results found using the EPRI (Reference 2.5S.2-12) and Peninsular Range (Reference 2.5S.2-47) strain dependency curves was negligible due to the very low level of shear strain in the soil layers. The EPRI set of soil strain dependency curves has been adopted for the base site model. A final sensitivity analysis also compared results of site responses obtained from profiles with different depths (1500 ft to 3500 ft, 457 m to 1066 m) to demonstrate that the truncation of the soil column does not affect the site response results over the frequency range of interest. Comparison of the results obtained from the profiles with different depths shows that the acceleration response spectra (ARS) amplification values within the frequency range of interest are very similar for all profiles. Based on the results of this comparison, a base profile truncated at 2500 +/- 500 ft (762 m) was adopted for the site response analyses of STP 3 & 4.

As described in Subsection 2.5S.4.7, Resonant Column Torsional Shear (RCTS) testing was delayed and the preliminary analysis for the development of site specific amplification factors was conducted using measured wave velocity profiles combined with published shear modulus and damping degradation curves. Results from five RCTS tests have been obtained and are discussed in Subsection 2.5S.4.7.3.3. Comparisons of these results with the generic EPRI curves selected for the corresponding soil layers in the base case soil column model demonstrate good correlation up to 10-2% strain (Reference Figures 2.5S.4-62 through 2.5S.4-64). Some divergence from the selected EPRI values above 10-2% strain can be observed for the samples from layers M-Sand and N-Sand (Reference Figures 2.5S.4-62 and 2.5S.4-63, respectively). For Substratum N-Clay (Reference Figure 2.5S.4-64), which presents data from 3 samples taken at different depths, the measured values straddled the assumed curves, dependent in part on the test confining pressure.

The soil column was truncated at a depth of 8100 ft (2469 meter). This depth was selected such that the resulting soil column captures the site response in the range of frequency of interest, greater than 0.1 Hertz. The natural soil column frequency was therefore calculated, starting from the best estimate shear-wave velocity profile, as shown in Figure 2.5S.2-35a, for the full soil column and confirmed to be less than 0.1 Hertz at 8100 ft depth.

As described in Subsection 2.5S.2.5.2, the soil properties for each layer were randomized to account for the inherent natural variability of soil deposits, as well as the (epistemic) uncertainty associated with the choice of curves for variation of shear modulus and damping with strain level. Therefore, the actual site response analysis comprised a range of soil properties for each layer, and in particular, a range of initial small strain shear modulus and degradation curves. Because of different properties in each of the randomized profiles, the site response analysis generated a range of results, as reported in Subsection 2.5S.2.5.4. As more RCTS tests are completed, the site-specific curves describing changes in shear modulus and damping with strain level may differ from those assumed in the analysis. However, the small strain shear modulus will remain unchanged. Given the reasonable, but also wide range of strain-dependent soil properties used for the randomization study, the effect of using site-specific RCTS data on soil amplification is expected to be small. This is particularly true considering that the sensitivity analysis described above clearly demonstrated that the use of EPRI curves rather than the Peninsular curves had little impact on site response, due to the low level of strains in the soil layers.

In addition, recognizing the margin between the site-specific GMRS described in Subsection 2.5S.2.6 (Figure 2.5S.2-52), and the RC-1-60, 0.3g CSDRS, it is expected that when the site-specific GMRS has been updated using all site-specific RCTS results, the GMRS will remain bounded by the CSDRS.

#### **2.5S.2.5.2 Site Properties Representing Uncertainties and Correlations**

To account for variations in shear-wave velocity across the site, 60 artificial profiles were generated using the stochastic model discussed in Reference 2.5S.2-50, with some modifications to account for conditions at the STP 3 & 4 site. These randomized profiles represent the truncated soil column from the top of bedrock with shear-wave velocity of 9200 feet per second (fps) to the ground surface. This model uses as inputs the following quantities:

- A shear-wave velocity profile for the upper 600 feet (182 m) of soil, which is equal to the base-case soil profile described above.
- A weighted average of the three deep (600 ft to 2500 ft, 182 m to 762 m) shear wave velocity profiles with the weighting values obtained from Reference 2.5S.2-48. A shear-wave velocity profile for the deeper soil column at depths greater than 600 feet (182 m) obtained from available deep sonic log data.
- The standard deviation of  $\ln(V_s)$  (the natural logarithm of the shear-wave velocity) as a function of depth, which was developed using available site and regional data (See Subsection 2.5S.4).

- The correlation coefficient between  $\ln(V_s)$  in adjacent layers, which is taken from generic studies, using the inter-layer correlation model for category US Geological Survey "C" soils (Reference 2.5S.2-50).
- The probabilistic characterization of layer thickness consists of a function that describes the rate of layer boundaries as a function of depth. This study used a generic form of this function, taken from Reference 2.5S.2-50 (Reference 2.5S.2-50), and then modified to allow for sharp changes in the adopted base-case velocity profile.
- The profiles of the median and plus/minus one standard deviation of the shear wave velocity profile are shown in Figure 2.5S.2-35b for the upper 1000 ft (Figure 2.5S.2-35). The variation was used in the randomization of the shear wave velocity profile.
- The assigned depth to bedrock of 8,100 ft to ensure the site response is captured, which is randomized about the depth of 2500 ft  $\pm$  500 ft (762 m  $\pm$  152 m) based on result of the comparative study of truncated profiles. Note that Subsection 2.5S.4.7.2.2.1 discusses that the shear wave velocity of 9200 ft/s is modeled at a depth of approximately 2500 ft (762 m). This value is taken as the base case or median depth. Depth to bedrock is characterized by a uniform distribution over the interval of 2500 ft (762 m), plus or minus 500 ft (152 m). Because bedrock occurs at a large depth, the specific details of modeling uncertainty in this depth are not critical to the calculation of site response in the frequency range of interest, greater than 0.1 Hertz.
- Median values of shear stiffness ( $G/G_{MAX}$ ) and damping for each geologic unit are described in Subsection 2.5S.4. Uncertainties in the strain-dependent properties for each soil unit are characterized using the values in Reference 2.5S.2-51. Figures 2.5S.2-37 and 2.5S.2-38 illustrate the shear stiffness and damping curves generated for one of the geologic units, Stratum MC, described in Subsection 2.5S.4.

Figure 2.5S.2-36 illustrates the 60  $V_s$  profiles generated, using the median, logarithmic standard deviation, and correlation model described above. These profiles include variation in depth to bedrock. The same figure compares the median of these 60  $V_s$  profiles to the median  $V_s$  profile described in the previous section, indicating good agreement.

This set of 60 profiles, consisting of  $V_s$  versus depth, depth to bedrock, stiffness, and damping, are used to calculate and quantify site response and its uncertainty, as described in the following sections.

### **2.5S.2.5.3 Correction of Damping for Scattering Effects to Maintain Total Site Kappa**

The process of the randomization of soil velocity profiles introduces additional scattering of upward propagating shear waves (S-waves) in such a manner that the median response of all randomized profiles is lower than the response obtained from the analyses of the median profile. These scattering effects are accounted for by decreasing the damping value of the deep soil layers in the randomized profiles by 15%. Due to this modification, the

mean (log-average) damping value of deep soil layer changes from 1.26% to 0.60% to 1.09% and the median values of total kappa ( $\kappa$ ) coefficient of site is reduced by 0.0023 to 0.005 sec. The modification has a very small effect on the variation of the randomized kappa ( $\kappa$ ) values as measured by the presented log standard deviation.

#### 2.5S.2.5.4 Site Response Analyses

The site response analysis performed for the STP 3 & 4 site uses Random Vibration Theory (RVT) (References 2.5S.2-52 and 2.5S.2-53) with the following assumptions:

- Vertically-propagating shear waves are the dominant contributor to site response
- An equivalent-linear formulation of soil nonlinearity is appropriate for the characterization of site response

These are the same assumptions that are implemented in the SHAKE program (Reference 2.5S.2-54) and that constitute standard practice for site-response calculations. In this respect, RVT and SHAKE solve the same problem, but RVT works with ground-motion power spectral densities or response spectra (and its relation to peak values), while SHAKE works with individual time histories and their Fourier spectra.

The RVT site-response analysis requires the following additional parameters:

- Strong-motion duration. These are calculated from the mean magnitudes and distances from the deaggregation using values of crustal shear wave velocity and seismic stress drop typical of Eastern North America. The RVT methodology requires this parameter, but results are not very sensitive to it. These are calculated from the mean magnitudes resulting from deaggregation. Table 2.3.1 in Reference 2.5S.2-58 provides strong motion duration values as a function of magnitude. Accordingly, strong motion durations were assigned for each of the cases considered ( $10^{-4}$  and  $10^{-5}$  annual frequencies, HF and LF smooth spectra), presented in Table 2.5S.2-20. Parametric studies during the site response analysis showed that the effect of this parameter is insignificant. A value of 10 seconds is used.
- Effective strain ratio. A value of 0.65 is used. Effective strain ratio is defined as the ratio between the peak acceleration of earthquake time history and the equivalent harmonic wave going through the soil layers (Reference 2.5S.2-55).

Figure 2.5S.2-39 shows with thick red lines the logarithmic mean and standard deviation of site amplification factors at ground surface from the analysis analyses of the 60 modified random profiles with the  $10^{-4}$  LF input motion. As would be expected due to the large depth of sediments at the site, amplifications are largest at low frequencies (below 2-3 Hz) and small de-amplification occurs at high frequencies because of soil damping. The maximum strains in the soil column are low for this motion, and this is shown in Figure 2.5S.2-40, which plots the maximum strains versus depth that are calculated for the 60 profiles and their logarithmic mean (in red thick line). The logarithmic mean of maximum strains is less than 0.025% to 0.03%. The maximum strain calculated from the analyses of all profiles is 0.055% to 0.05% in the upper 600 feet (182 m) of soil. The maximum strains in the deep soil

layer at depths below 600 feet (182 m) are very small and do not exceed value of ~~0.015%~~0.02%.

Figure 2.5S.2-41 and Figure 2.5S.2-42 show similar plots of amplification factors and maximum strains obtained from the analysis analyses with  $10^{-4}$  HF motion. The maximum strain results show that the soil column exhibits a lower level of straining under this earthquake with maximum strains being less than ~~0.02%~~0.025%. Figure 2.5S.2-43 through Figure 2.5S.2-46 show comparable plots of amplification factors and maximum strains from the analyses performed with the  $10^{-5}$  input motion, both LF and HF. For this higher motion, larger maximum strains are observed, but the maximum logarithmic mean does not exceed ~~0.1%~~0.11%. From all of the 60 profiles, a maximum strain of ~~0.45%~~0.19% is calculated in the upper 600 feet (182 m) of soil. The maximum strain in the deep soil layers is very small, less than ~~0.05%~~0.06%.

Comparison of the profiles of logarithmic mean maximum strain in Figure 2.5S.2-47 clearly indicates that response of the site under the LF motions is stronger than under HF motions. Figure 2.5S.2-48 shows the logarithmic mean profiles for the strain-compatible damping that is a measure of energy dissipation in the soil profile during the shaking. Corresponding to the strains, a maximum damping value of ~~6.8%~~3.4% in the upper 600 feet (182 m) of soil is calculated for the analyses with the  $10^{-5}$  LF motion. The strain compatible damping calculated for is the  $10^{-4}$  LF motion small and does not exceed ~~3.5%~~1.9%. The small strain-compatible damping results in relatively small de-amplification of the site response at high frequencies.

A comparison of log-mean soil amplification factors at the ground surface level for LF and HF  $10^{-4}$  and  $10^{-5}$  input motions is shown in ~~Figure 2.5S.2-49~~Figure 2.5S.2-49a. As shown in this figure, the amplifications at  $10^{-4}$  level of input motion between the LF and HF input motions are about the same up to 7 Hz. De-amplification occurs at higher frequencies ~~is small particularly for the LF input motion,~~ larger than 10 Hz, followed by amplification of the peak ground acceleration (about 1.6) at high frequencies (above ~~80~~40 Hz). The amplification due to  $10^{-5}$  level of input motion follows the same trend compared to the amplification due to  $10^{-4}$  motion indicating limited extent of soil nonlinearity in the soil column. ~~The corresponding amplified ARS at ground surface are presented in Figure 2.5S.2-49b.~~

~~The corresponding numerical values of the soil amplification factors are tabulated in Table 2.5S.2-18 and 2.5S.2-19.~~

### 2.5S.2.6 Ground Motion Response Spectra

The following site-specific supplement addresses COL License Information Item 2.2.

The GMRS ground motion was developed starting from the  $10^{-4}$  and  $10^{-5}$  HF and LF rock UHRS shown in Figures 2.5S.2-33 and 2.5S.2-34. Site response was calculated for each of these rock input motions. Figure 2.5S.2-50 shows the resulting logarithmic mean spectra for surface conditions for each of these input rock motions; see Tables 2.5S.2-18 and 2.5S.2-19 for sampled numerical values of these rock response spectra. The broad-banded LF motion dominates the site response for the  $10^{-4}$  rock input motion, but for  $10^{-5}$  the HF rock motion indicates higher response in the frequency range 12.5 to 3.3 Hz. The envelope spectra for  $10^{-4}$  and  $10^{-5}$  were determined from these individual results, and these

envelope spectra were smoothed with a running average filter to smooth out peaks and valleys that are not statistically significant. These envelope spectra are shown in Figure 2.5S.2-51; see Tables 2.5S.2-18 and 2.5S.2-19 for sampled numerical values of these rock response spectra.

This procedure corresponds to Approach 2A in NUREG/CR-6769 (Reference 2.5S.2-2), wherein the rock UHRS (for example, at  $10^{-4}$ ) is multiplied by a mean amplification factor at each frequency to estimate the  $10^{-4}$  site UHRS.

The low-frequency character of the spectra in Figures 2.5S.2-34 and 2.5S.2-50 reflects the low-frequency amplification of the site. This is a deep soil site and there is a fundamental site resonance at about 0.6 Hz, with a dip in site response at about 0.7 Hz, and this dip occurs for all 60 of the site profiles that were used to characterize the site profile. As a result, there is a dip in the site spectra for  $10^{-4}$  and  $10^{-5}$  at 0.7 Hz that reflects the site characteristics.

The horizontal GMRS was developed from the horizontal UHRS using the approach described in ASCE/SEI Standard 43-05 (Reference 2.5S.2-56) and RG 1.208. The ASCE/SEI Standard 43-05 approach defines the GMRS using the site-specific UHRS, which is defined for Seismic Design Category SDC-5 at a mean  $10^{-4}$  annual frequency of exceedance. The procedure for computing the GMRS is as follows.

For each spectral frequency at which the UHRS is defined, a slope factor AR is determined from:

$$AR = SA(10^{-5})/SA(10^{-4}) \quad \text{Equation 2.5S.2-8}$$

STP COLA Part 2, Tier 2, Subsection 2.5S.4.7, "Response of Soil and Rock to Dynamic Loading," will be revised as shown below:

#### **2.5S.4.7.1 Site Seismic History**

The seismic history of the area and of the site, including any prior history of seismicity, and evidence of liquefaction or boils is addressed in Subsections 2.5S.1.1.4.4.5 and 2.5S.1.2.6.4.

#### **2.5S.4.7.2 P- and S-Wave Velocity Profiles**

Given the extreme thickness of sediments at the site (refer to Subsection 2.5S.4.1) compared to the depth of compressional and shear wave velocity measurements made during the STP 3 & 4 subsurface investigation (to approximately 600 feet below ground surface), additional information was required to complete the velocity profile for the site. Velocities in the upper 600 feet were measured at the site, while velocities deeper than 600 feet were obtained from available references. Additional discussion follows.

### 2.5S.4.7.2.1 Seismic Velocity in the Upper 600 Feet

Geophysical measurements in the upper 600 feet at STP 3 & 4 were obtained by suspension P-S velocity logging methods, and by seismic CPT methods, as discussed in Subsection 2.5S.4.4.2. An average shear wave velocity profile for the upper 600 feet at STP 3 & 4 is shown on Figures 2.5S.4-45, 2.5S.4-46, and 2.5S.4-47. Average shear wave velocities ( $V_s$ ), Poisson's ratios ( $\mu$ ), and related parameters are summarized in Table 2.5S.4-27.

Suspension P-S velocity logging measurements were made at 10 borings, five each at the STP 3 area and the STP 4 area, with depths ranging from approximately 200 feet to 600 feet below ground surface, and at locations shown on Figure 2.5S.4-2. Seismic CPT measurements were made at ~~five six~~ CPTs, three at the STP 3 area and ~~two three~~ at the STP 4 area, with depths ranging from approximately 65 feet to 95 feet below ground surface, and at locations shown on Figure 2.5S.4-2. The suspension P-S logging data and the seismic CPT data are contained in Reference 2.5S.4-2. As shown on Figures 2.5S.4-40 and 2.5S.4-41, the trends in  $V_s$  profiles between the STP 3 area and the STP 4 area are generally consistent. Also for comparison, the  $V_s$  profiles obtained previously for STP 1 & 2 (Reference 2.5S.4-3) to a depth of approximately 300 feet below ground surface are shown along with the  $V_s$  profiles obtained from the STP 3 & 4 subsurface investigation on Figures 2.5S.4-43 and 2.5S.4-44.

In general, comparison of measured STP 1 & 2  $V_s$  results with those obtained from the STP 3 & 4 subsurface investigation indicate relatively consistent results, ignoring variations of about  $100\pm$  feet/second, except between approximately El. -40 feet to -105 feet, where greater differences of the order of 300 to 400 feet/second are noted. Note that this comparison is only for the upper approximately 300 feet of soils at STP 3 & 4, as the STP 1 & 2 data (shown on Figures 2.5S.4-43 and 2.5S.4-44) only extended to approximately 300 feet below ground surface.

As noted above, design/average shear wave velocity ( $V_s$ ) and Poisson's ratio ( $\mu$ ) values are summarized in Table 2.5S.4-27. Note that these design/average values were developed considering the variation in strata top/base elevations and thicknesses from boring-to-boring and from CPT-to-CPT. Note also that Sub-stratum J Sand was found to contain four separate interbedded sub-strata of sands and/or silts at various depths (i.e., Sub-stratum J Interbed 1 [sand or silt], Sub-stratum J Sand 1, Sub-stratum J Interbed 2 [sand or silt], and Sub-stratum J Sand 2) which were additionally discontinuous between boring locations. For developing Sub-stratum J Sand design/average values, shear wave velocity measurements obtained for the various interbedded sands and silts were fitted to a single sand/silt sub-stratum occurring between the two clay sub-strata (i.e., Sub-stratum J Clay 1 and Sub-stratum J Clay 2).

### 2.5S.4.7.2.2 Seismic Velocity Below 600 Feet

The soil sediments at STP 3 & 4 extend well below the 600 feet maximum depth of the STP 3 & 4 subsurface investigation. Additional subsurface information was sought to characterize the site conditions below this depth.

#### **2.5S.4.7.2.2.1 Soil Shear Wave Velocity Profile**

The upper 600 feet at STP 3 & 4 were investigated using borings, CPTs, and geophysical logging methods, and the design/average velocity profile to that depth is described in Subsection 2.5S.4.7.2.1. Between approximately 600 feet below ground surface and 2620 feet below ground surface, subsurface and shear wave velocity information was taken from the STP 1 & 2 UFSAR (Reference 2.5S.4-3). According to that reference, the subsurface deeper than 600 feet below ground surface consists of alternating layers of very stiff to hard clay (with some claystones and siltstones) and very dense, fine to silty fine sand. The claystones and siltstones occur at depths greater than approximately 880 feet below ground surface, with the frequency of their occurrence increasing with depth. Refer to Subsection 2.5S.4.1 for a brief description of geologic conditions at greater depths, a key point being that the top depth of pre-Cretaceous bedrock ("basement rock") has been estimated to occur at approximately 34,500 feet below ground surface (Reference 2.5S.4-4).

Reference 2.5S.4-4 also contains deep shear wave velocity profiles developed for a later-stage review of the STP site, among others. These profiles increase in shear wave velocity to a depth of approximately 2500 feet below ground surface and then maintain a common value of  $V_s$  between 2500 feet and 5000 feet depths. According to the Reference 2.5S.4-4, these profiles were based on site-specific cross-hole measurements in the uppermost approximately 250 feet and were then attached to the deeper and more generic "Mississippi embayment lowlands profile," which is described in more detail in the reference. The resulting composite  $V_s$  profiles are reproduced and shown on Figure 2.5S.4-57. Note that the details of this figure are truncated at El. -3250 feet, corresponding to a depth of approximately 3280 feet below ground surface, or 1 kilometer. Three shear wave velocity profile cases, M1P1, M1P2, and M1P3, are provided on the figure. The three profiles in Figure 2.5S.4-57 all show an increase in shear wave velocity to 9285 feet/second at a depth of approximately 2500 feet. Numerical values from the three shear wave velocity profiles versus depth, between 600 feet and 3280 feet below ground surface, or 1 kilometer, are summarized in Table 2.5S.4-28. Soil unit weight information is limited deeper than 600 feet, with available information from the STP 1 & 2 UFSAR (Reference 2.5S.4-3) given in Table 2.5S.4-29. Note that for completeness, Table 2.5S.4-29 also provides the selected values of unit weight for the upper 600 feet of soils from the STP 3 & 4 subsurface investigation.

#### **2.5S.4.7.2.2.2 Bedrock Shear Wave Velocity Profile**

To assess the  $V_s$  profile at substantially greater depth, a search was made of geophysical logging results (especially sonic logging) made for existing oil wells in the STP site vicinity. Three such wells were selected (LL3341, LL4537, and LL4987) from the available information, having the deepest sonic logging results (to a maximum of approximately ~~15,600-19,900~~ feet below ground surface). ~~An initial~~ Conversion of the sonic logging data to shear wave velocities showed generally good agreement with the shear wave profiles presented on Figure 2.5S.4-57 down to depths of approximately 2,500 feet. ~~These data will be further reduced, and the results/comparisons provided at a later date (refer to the statement on COM 2.5S-1 at Subsection 2.5S.4.7).~~

The average shear wave velocity obtained from converting the data in the three sonic logs was used for the deep layers as input to the site response analysis. Based on the conversion, in general, the shear wave velocity profile is as follows:

- At a depth of 2,500 feet the sonic logging data showed the shear wave velocity to be in the range of 2,900 to 3,200 feet/second, consistent with the results on Figure 2.5S.4-57. This range continues to a depth of 3,000 feet;
- Increases from 3,000 feet/second at a depth of 3,000 feet to 5,000 feet/second at 6,000 feet depth;
- Decreases to around 3,500 feet/second at an 8,000 feet depth;
- Increases linearly to 5,500 feet/second at an 18,000 feet depth; and
- Increases to about 6,500 feet/second just beyond 18,000 feet depth, then falls back to 5,000 feet/second at a 19,000 feet depth.

### 2.5S.4.7.3 Static and Dynamic Laboratory Testing

Extensive static laboratory testing of representative soil samples obtained from the STP 3 & 4 subsurface investigation were conducted, with results described in detail in Subsection 2.5S.4.2.

Dynamic laboratory testing was performed, consisting of Resonant Column Torsional Shear (RCTS) tests, to obtain data on shear modulus and damping ratio characteristics of site soils over a wide range of strains, is now in progress. A total of 18-16 undisturbed soil samples, from depths of 10 feet to 590 feet below ground surface, were assigned for subjected to RCTS testing. Results from five of those assigned RCTS tests are available at this time and are discussed briefly below (Subsection 2.5S.4.7.3.3). In the interim a summary of the samples tested is included in Table 2.5S.4-31. Prior to these tests being completed and the results becoming available, the shear modulus degradation and damping ratio versus shear strain curves from the available literature were used for dynamic soil properties characterization. Once all assigned RCTS tests have been the laboratory testing was completed, an evaluation will be was made, comparing the laboratory of the RCTS test-derived modulus reduction and damping curves and a comparison made with the literature-derived curves, with the selected (literature) curves (refer to the statement on COM 2.5S.4 at Subsection 2.5S.4.7). Refer to Subsection 2.5S.2 for additional discussion.

In the absence of final RCTS test results, shear modulus degradation and damping ratio curves selected from the available literature for the various STP 3 & 4 soil strata are discussed below. A brief review of the five available laboratory RCTS test results is also provided.

A total of 16 undisturbed soil samples were assigned for RCTS testing to measure shear moduli and damping ratios for selected site soils across a wide range of strains. The results of completed RCTS tests are discussed here and compared with the selected (literature) curves.

**2.5S.4.7.3.1 Selected Shear Modulus Degradation Curves for Soils from Literature**

Generic shear modulus degradation curves for cohesionless soil or sub-strata strata B, C, E, H, J Sand/Silt, K Sand/Silt, M, and N Sand were developed from Reference 2.5S.4-49, based on stratum depths. The depths of soil strata or sub-strata at approximate mid-thicknesses, summarized in Table 2.5S.4-30, were used to develop strata-specific curves. The specific/recommended curves for the above-noted cohesionless soil strata are shown on Figure 2.5S.4-58, with numerical values given in Table 2.5S.4-324. An alternate set of curves for cohesionless soil strata, "Peninsular Range" curves (Reference 2.5S.4-50), were also evaluated, and are similarly shown on Figure 2.5S.4-58, with numerical values given in Table 2.5S.4-324. Note that these latter curves provide a range of values that can allow for overconsolidation and other variations.

Generic shear modulus degradation curves for cohesive soil strata A, D, F, J Clay, K Clay, L, and N Clay were similarly developed from Reference 2.5S.4-49, based on strata plasticity indices (PI). For cohesive soil strata occurring at depths greater than approximately 100 feet, an increase in the PI value was taken, equivalent to the next higher PI reference curve shown in Reference 2.5S.4-49 (as per Reference 2.5S.4-51). As an example, for a clay stratum deeper than 100 feet and having PI=10%, the next higher reference curve for PI=30% was used in selecting the shear modulus degradation relationship. The PI value (maximum) was capped at 70%. The specific/recommended curves for the above-noted cohesive soil strata are shown on Figure 2.5S.4-59, with numerical values given in Table 2.5S.4-324.

**2.5S.4.7.3.2 Selected Damping Ratio Curves for Soils from Literature**

Generic damping ratio curves for cohesionless soil strata B, C, E, H, J Sand, K

Sand/Silt, M, and N Sand were developed from Reference 2.5S.4-49, based on strata depth. The specific/recommended curves for the above-noted cohesionless soil strata are shown on Figure 2.5S.4-60, with numerical values given in Table 2.5S.4-332. An alternate set of curves for cohesionless soil strata, "Peninsular Range" curves (Reference 2.5S.4-50), were also evaluated, and are similarly shown on Figure 2.5S.4-60, with numerical values given in Table 2.5S.4-332.

Generic damping ratio curves for cohesive soil strata A, D, F, J Clay, K Clay, L, and N Clay were also developed from Reference 2.5S.4-49, based on strata plasticity indices (PI). For cohesive strata occurring at depths greater than approximately 100 feet, an increase in the PI value was taken, as noted above (as per Reference 2.5S.4-51). The specific/recommended curves for the above noted-cohesive soil strata are shown on Figure 2.5S.4-61, with numerical values given in Table 2.5S.4-332.

Note that in the referenced figures and tables, damping ratios were provided at values exceeding 15%, although, damping is frequently cut off at this value. For the purpose of dynamic analyses, damping ratio is limited to 15%, and the portions of the referenced figures and tables above this value are not considered.

### 2.5S.4.7.3.3 Comparison of Selected and Measured Shear Modulus Degradation and Damping Ratios for Soils

As described previously, in the absence of site specific dynamic test results, shear modulus degradation and damping ratio curves for site soils were selected from the available literature, as given in Tables 2.5S.4.31 and 2.5S.4.32 and as shown on Figures 2.5S.4.58 through 2.5S.4.61. A total of 18 undisturbed soil samples were assigned for RCTS testing to measure shear moduli and damping ratios for selected site soils across a wide range of strains. The results of five completed RCTS tests are discussed here and compared with the selected (literature) curves. The results of the remaining assigned tests are pending. Note that the results of the five available RCTS tests were for soils from three main strata, namely, Stratum M, (one test) Sub-stratum N Clay (one test on N Clay 1, one test on N Clay 2, and, one test on N Clay 4), and Sub-stratum N Sand (one test on N Sand 2). A summary of the results of the available tests is given in Table 2.5S.4.33, with comparisons of individual test results to selected (literature) curves given on Figures 2.5S.4.62 through 2.5S.4.64. Note that the RCTS test results shown are for a wide range of confining stresses (i.e., from less than 100 pounds per square inch [psi] to over 400 psi) and frequencies (i.e., from 0.5 Hz to over 80 Hz), therefore, some spread in the results should be expected. The following initial observations can be made from the available RCTS test results:

- For the tests made on samples from Stratum M and Sub-stratum N Sand, up to a shear strain level of approximately  $10^{-2}\%$ , there is very close agreement between the measured test results and the selected (literature) shear modulus degradation and damping curves. At shear strain levels above approximately  $10^{-2}\%$ , the differences widen, indicating either matching or higher measured shear moduli and lower measured damping ratios than those portrayed by the selected (literature) curves.

- The spread in results appears more pronounced in the tests made on the three samples from Sub-stratum N Clay (Figure 2.5S.4.64), which were taken from a range of depths spanning approximately 145 feet. The measured test results here show somewhat different responses at different depths. Note however, that the selected (literature) curve falls within the mid-range of the RCTS data.

The above observations are based on limited RCTS test results. While the available test results, in some cases, indicate a somewhat different soil response than those selected for shear strain levels exceeding approximately  $10^{-2}\%$ , any necessary modifications to the dynamic soil model should await the completion of the RCTS testing program, and a comprehensive review of all the RCTS test results (refer to the statement on COM-2.5S-1 at Subsection 2.5S.4.7). Refer to Subsection 2.5S.2 for additional discussion.

A summary of the results of the RCTS tests is provided in Table 2.5S.4.34, with comparisons of individual test results to the selected (literature) curves given on Figures 2.5S.4.62 through 2.5S.4.68. Note that the RCTS test results shown are for a wide range of confining stresses (i.e., from less than 100 pounds per square inch [psi] to over 400 psi) and frequencies (i.e., from 0.5 Hz to over 80 Hz), therefore, some spread in the results should be expected.

Details of the RCTS results are contained in Reference 2.5S.4-2A. The soil samples subjected to RCTS tests were divided into the following categories:

- 1) Sand
  - a) Deep sand with depth greater than 105 ft
  - b) Shallow sand with depth no more than 105 ft
- 2) Clay
  - a) High PI clay with PI greater than 30
  - b) High PI clay with PI no more than 30
- 3) Silt

#### **2.5S.4.7.3.4 Comparison of Selected and Measured Shear Modulus Degradation for Soils**

The shear modulus degradation ( $G$ ) curves for all the sand samples are presented in Figure 2.5S.4-62, along with the EPRI curves derived versus depth in Reference 2.5S.4-50. Note that the results plotted on Figures 2.5S.4-62 through 2.5S.4-65 are those results obtained using a confining pressure equal to or very close to the in-situ confining pressure. Figure 2.5S.4-62 shows that at the same strain level the normalized shear modulus ( $G/G_{max}$ ) generally increases with depth. The one exception is sample B306-UD3 located at 75 ft depth, which is considered an outlier. The  $G$  curves for the deep sand samples are also presented in Figure 2.5S.4-63, along with the average of the deep curves, and the EPRI curves. The  $G$  curves of the deep soil samples generally agree with each, and their average is close to the EPRI curve for depth = 500 - 1000 ft. Figure 2.5S.4-62 shows that soil sample B-306-UD-6 located at the depth of 104.7 ft is consistent with the EPRI curve for depth = 250 - 500 ft. Therefore, it is recommended that the following shear modulus degradation curves be used for sand strata at the STP site:

- For sands located at depths greater than 100 ft, use the EPRI curve for depth = 500 - 1000 ft
- For sands located at depths less than 100 ft, use the EPRI curve for depth = 250 - 500 ft

The shear modulus degradation curves for all the high PI clay samples are presented in Figure 2.5S.4-64, along with their average, which is quite close to Vucetic & Dobry (1991) curve for PI = 100 (Reference 2.5S.4-65). The shear modulus degradation curves for the low PI clay sample and the silt sample are presented in Figure 2.5S.4-65. Based on comparison between the test curves and the published curves, it is recommended that the following shear modulus degradation curves be used for clay and silt:

- For clays with PI greater than 30, use the Vucetic & Dobry curve for PI = 100
- For clays with PI less than 30, use the Vucetic & Dobry curve for PI = 50
- For silt, use the EPRI curve for PI = 50

### 2.5S.4.7.3.5 Comparison of Selected and Measured Damping Ratio Curves for Soils

The damping ratio (D) curves for all the sand samples subject to TS tests are presented in Figure 2.5S.4-66, along with the average of the curves. The results consistently show that the D curves are close to the EPRI curve for depth = 500 - 1000 ft. Therefore, it is suggested that the following D curve be used for all the sands:

- For all sands, use EPRI curve for depth = 500 - 1000 ft

The D curves for high PI clay are presented in Figure 2.5S.4-67, along with their average, which is quite consistent with the Vucetic & Dobry curve for PI = 200.

- For clays with PI greater than 30, use the Vucetic & Dobry curve for PI = 200

The D curves for the low PI clay sample and the silt sample are presented in Figure 2.5S.4-68. These curves do not consistently follow any single EPRI or Vucetic & Dobry curve. At strains below about 0.005%, the test curves are close to the Vucetic & Dobry curve for PI = 200. However, at higher strains, the slope for both tests becomes steeper and is closer to the EPRI PI = 50 or PI = 70 curves.

- For low PI clay and silt samples, use Vucetic & Dobry curve for PI = 200 up to strains of 0.005% and use EPRI interpolated PI = 60 curve for strains above 0.05%.

### 2.5S.4.7.3.6 ~~2.5S.4.7.3.4~~ Shear Modulus and Damping for Rock

Refer to Subsection 2.5S.4.1 for a brief description of geologic conditions at depths below approximately 600 feet below ground surface, a key point being that the top depth of pre-Cretaceous bedrock ("basement rock") has been estimated to occur at approximately 34,500 feet below ground surface (Reference 2.5S.4-4).

Refer also to Subsection 2.5S.4.7.2.2.1 for discussion of deep shear wave velocity profiles pertinent to the STP site and derived from information contained in Reference 2.5S.4-4.

It should be noted that hard rock is considered to have damping, but is not strain dependent. For the STP 3 & 4 work, a damping ratio of 0.2% was adopted for bedrock, and bedrock shear modulus was considered to remain constant (i.e., no degradation), in the shear strain range of  $10^{-4}$  % to 1%.

### 2.5S.4.7.3.7 ~~2.5S.4.7.3.5~~ Dynamic Properties of Structural Fill

Some major structures (e.g., the Reactor Buildings, the Radwaste Buildings, and the RSW Tunnels) require over-excavation and the placement of either concrete fill or structural fill below their foundations. Refer to Subsection 2.5S.4.5 for structural fill requirements.

### 2.5S.4.7.4 Small Strain Shear Modulus Estimation

With shear wave velocity and other parameters established, small strain shear modulus values can be calculated from Equation 2.5S.4-6. Note that shear wave velocity values for use in the equation are given in Tables 2.5S.4-27 and 2.5S.4-28, and unit weight values for use in the equation are given in Table 2.5S.4-29. Refer to Subsection 2.5S.4.2.2 for a

stratum-by-stratum discussion of the derivation of shear modulus (G) and other geotechnical engineering parameters for use in design.

**2.5S.4.7.5 Seismic Parameters for Liquefaction Potential Analysis**

Using the site-specific soil column extended to ground surface, the amplification factor, and the performance-based hazard methodology employed to develop the GMRS (refer to Subsections 2.5S.2.5 and 2.5S.2.6), a peak horizontal ground surface acceleration of 0.10g and a Moment Magnitude 7.7 earthquake was selected for use in liquefaction potential analysis. Refer in particular to Subsection 2.5S.2, Table 2.5S.2-17 entitled "Controlling Magnitudes and Distances from Deaggregation," regarding selection of the earthquake magnitude for use in liquefaction potential analysis.

**RAI 02.05.02-20****Question:**

You summarized Mid America Trench sensitivity analysis in FSAR Com 2.5S-1. Please provide detailed contents on this sensitivity analysis, including detailed source characterization, attenuation relationships and other related information.

**Response:**

The following supplemental information is provided for the discussion of "Middle America Trench Seismic Hazard Sensitivity," which was summarized in the response to FSAR Com 2.5S-1 (U7-C-STP-NRC-080070, dated December 15, 2008).

***Seismic Source Model***

The Middle America Trench (MAT) source model used in the STP 3 & 4 sensitivity analysis is a simplified model that accounts for characteristic interplate subduction earthquakes from the MAT adjacent to Mexico. The MAT source model was developed following a SSHAC level 1 process (Budnitz et al., 1997), and as such the MAT source characterization includes epistemic uncertainty in the following characteristics of the MAT: segmentation, variations in subducting plate geometry, up- and down-dip limits of seismogenic rupture, relative convergence rate between the subducting and overriding plates, amount of seismic coupling on the plate interface, and the characteristic magnitude of interplate events.

In the source model the MAT is divided into the four distinct segments, shown on Figure 1, based on: 1) variations in the age of subducted oceanic crust, 2) dip of the subducting plate, 3) extent of historic interplate earthquake ruptures, and 4) the presence or absence of fracture zones and ridges on the subducting plate (Mann et al., 2006; Núñez-Cornú et al., 2002; Pardo and Suarez, 1995; Santoyo et al., 2005; Yoshioka et al., 2004). The historical record of MAT seismicity demonstrates that the MAT has been characterized by single-segment ruptures approximately corresponding to these four segments (Santoyo et al., 2005), but many in the research community believe that most subduction zones, including the MAT, are capable of large multiple-segment ruptures (Ammon et al., 2005; Lay et al., 2005; McCaffrey, 2008). Therefore, the MAT source model includes the possibility of multiple-segment rupture. Specifically, three multiple-segment rupture scenarios are considered: rupture of 1) all of the segments from Michoacan to Chiapas; 2) the Michoacan and Guerrero segments; and 3) the Guerrero and Chiapas segments. The Jalisco-Rivera segment is not included in multiple-segment rupture scenarios because the Rivera plate behaves as an independent plate from the Cocos plate (Bird, 2003; DeMets and Traylen, 2000; DeMets and Wilson, 1997).

Earthquakes were modeled as occurring along the seismogenic portion of the subducting plate interface. Plate geometries (location and dip) for each segment of the MAT were determined from available published information including earthquake hypocenters, seismic reflection data, seismic refraction data, and gravity data (Currie et al., 2002; Kostoglodov et al., 1996;

Kostoglodov et al., 2003; Pardo and Suarez, 1995). The width of the seismogenic portion of the subducting plate interface was defined using commonly accepted thermal limits (Byrne et al., 1988; Hyndman and Wang, 1993; Hyndman et al., 1995; Moore and Saffer, 2001; Oleskevich et al., 1999) determined from the thermal models of Currie et al. (2002). The resulting seismogenic width is consistent with observations of Moho depth (Bandy et al., 1999; Iglesias et al., 2001; Manea et al., 2006) and earthquake focal depths (Pacheco et al., 1993; Tichelaar and Ruff, 1993).

A range of characteristic magnitudes for the MAT was considered. The lower-bound magnitude was generally based on the largest historical interplate earthquake for each segment, and the upper-bound was generally based on the largest physically reasonable earthquake given the geometry (i.e., rupture area) of the segments. Magnitudes based on rupture area followed Gregor et al. (2002) and used the relationships of Wells and Coppersmith (1994). The effect of epistemic uncertainty in plate dip and seismogenic width was propagated into uncertainty in the resultant magnitudes. The final magnitudes and weights for the various rupture segments and scenarios are (all magnitudes are  $M_w$ ): Jalisco to Rivera, 8.0 (0.2), 8.3 (0.6), 8.6 (0.2); Michoacan, 8.1 (0.2), 8.4 (0.6), 8.7 (0.2); Guerrero to Oaxaca, 7.9 (0.2), 8.3 (0.6), 8.7 (0.2); Chiapas, 7.9 (0.2), 8.2 (0.6), 8.5 (0.2); Michoacan to Chiapas, 8.6 (0.4), 8.85 (0.4), 9.1 (0.2). In general a weight of 0.2 was used for the largest observed magnitude and a combined weight of 0.8 was used for the magnitudes estimated from rupture area reflecting the belief that the observed magnitude is not the maximum magnitude for the MAT.

Recurrence rates for interplate earthquakes along the MAT were calculated using a moment budget for the MAT given the convergence rate and direction (DeMets et al., 1994; DeMets and Traylen, 2000; DeMets and Wilson, 1997; McCaffrey, 1993) and plate coupling ratio (the ratio of the amount of convergence recovered during earthquakes to the total convergence rate). In general coupling ratios are poorly constrained, so a range of coupling ratios was used based on global seismic moment studies and local geodetic studies (Azua and DeMets, 2002; Bird and Kagan, 2004; Frohlich and Wetzell, 2007; Iglesias et al., 2004; Kostoglodov et al., 2003; Kostoglodov et al., 2001; Larson et al., 2007; Larson et al., 2004; Pacheco et al., 1993; Yoshioka et al., 2004). The weighted coupling ratios for each segment are: 0.3 (0.2), 0.5 (0.5), 0.7 (0.2), 0.9 (0.1).

The final source model for the MAT is composed of two independent sources resulting in five rupture scenarios (Table 1) (Figure 2). The first source is the Jalisco-Rivera segment of the MAT. This segment is not capable of multiple-segment rupture, so it is a unique source and has only one source rupture scenario (Figure 2). The second source is the MAT from Michoacan to Chiapas. This source has the potential for multiple-segment rupture of the MAT and has four rupture scenarios: one single-segment and three scenarios considering the potential for multi-segment rupture. The potential for multiple-segment rupture is given a weight of 0.3 reflecting the potential, but historically unobserved, possibility of multiple segment rupture (Figure 2). Within the multi-segment rupture branch of the logic tree epistemic uncertainty in the relative frequency of single-segment vs. multi-segment ruptures is represented with three alternative models (Table 2): one model uses the historical earthquake record to estimate the minimum number of single segment earthquakes that occur along the Michoacan to Chiapas segment before a multi-segment rupture occurs, and the other two models are based on the expected

relative frequency of characteristic single and multi-segment earthquakes based on the expected magnitudes of those earthquakes and a Gutenberg-Richter relationship for magnitude recurrence (Kagan, 1999; McCaffrey, 2008; McGuire, 2004). The two Gutenberg-Richter models reflect epistemic uncertainty in the single- and multi-segment rupture magnitudes that are compared to determine the relative frequency. The third model has the lowest weight because it represents a model where there is relatively little difference in magnitude between a single- and multi-segment rupture suggesting the two rupture types occur with the essentially the same frequency, which is contraindicated by the historic earthquake record.

### **1 Hz Ground Motion Attenuation Model**

As stated in the response to FSAR Com 2.5S-1, “Given the large distance and the average crustal attenuation characteristics between the MAT and the project site, it was assessed that longer period motions would be most likely to contribute to the seismic hazard at the STP 3 & 4 site. For this reason, the sensitivity study focused on 1 Hz ground motion. Further, for the purpose of the sensitivity study, focus was placed on the subduction interface earthquakes, the source of earthquakes observed as large as nearly  $M \sim 8$  and arguably with the potential of being as large as  $M \sim 9$ . The sensitivity study required development of a seismic source model for the large magnitude MAT subduction interface earthquakes, as well as a long distance 1 Hz ground motion attenuation relationship.”

To perform the PSHA sensitivity analysis for MAT, an appropriate ground motion attenuation model had to be selected. This attenuation model for 1 Hz spectral frequency attenuation should be applicable for large interface subduction earthquakes at large distances on the order of 1,000 to 2,000 km to satisfy the site-specific conditions.

An assessment of seven published attenuation models for 1 Hz spectral acceleration attenuation from subduction zone interface earthquakes was performed. These relationships are based on both empirical ground motion recordings and/or synthetic modeled ground motion data. The list and description of the seven attenuation models that were considered in the analysis is given in Table 3. While only two of the published relations (both based on simulation ground motion data) were presented as applicable to the large distances needed for the PSHA sensitivity study, all seven were evaluated as to their median attenuation behavior over a magnitude range 6.5 to 8.5 and for distances out to 2,000 km. The median 1 Hz spectral acceleration attenuation curves from the seven candidate models are shown in Figure 3, Figure 4 and Figure 5 for magnitudes, 6.5, 7.5, and 8.5, respectively. The corresponding aleatory sigma values for each of the seven attenuation models are shown in Figure 6. Note that these aleatory sigma values are magnitude independent and span a range in values of approximately a factor of 2 in natural log units. Based on these plots the following conclusions were reached:

- The range in sigma values is about a factor of 2 (from about 0.5 to 1) in natural log units.
- The sigma values based on empirical data are typically larger than sigma values given for crustal earthquake attenuation models.
- The (Megawati et al., 2005) and (Pan et al., 2007) relationships, which are based on numerical simulations and not empirical data, give the smallest sigma values of less than

0.6. It was also noted that the (Pan et al., 2007) model has an additional 0.2 sigma value added to the regression sigma value based on the authors concern that the regression sigma underestimates the true aleatory sigma.

- The (Kanno et al., 2006) sigma is the largest with a value about 0.95 natural log units. This large uncertainty could be a consequence of not differentiating the shallow events in their database into crustal events and interface events.
- For the median attenuation curves shown in Figure 3, Figure 4 and Figure 5 as well as the aleatory sigma model given in Figure 6, the (Zhao et al., 2006) relationship gives an approximate average value for all of the models.

As a result of the comparison, a representative model (Zhao et al., 2006) among the suite of the seven considered relationships was chosen as the 1 Hz spectral acceleration ground motion for use in the MAT PSHA sensitivity analysis.

To capture the epistemic uncertainty a bounding value appropriate for this MAT PSHA sensitivity study was estimated. The epistemic uncertainty was computed for the suite of the four subduction zone attenuation models which are based on empirical ground motion data: (Youngs et al., 1997), (Atkinson and Boore, 2003), (Zhao et al., 2006), and (Kanno et al., 2006). For these four models, the computed epistemic values for magnitudes 6.5, 7.5, and 8.5, assuming equal weights between each of the four models are shown in Figure 7 for distances less than 300 km (solid lines), as well as the extrapolated values for longer distances for the three magnitude values (dashed lines). In addition to the empirically based subduction zone attenuation models, the computed epistemic uncertainty from the suite of CEUS ground motion models from the (EPRI, 2004) ground motion report is also plotted in Figure 7. For distances less than 300 km (i.e., the cut off distance of applicability for the subduction zone models based on empirical ground motion data), the epistemic values fall below the recommended bounding value of 0.75. Only for distances greater than approximately 600 km does the computed epistemic uncertainty approach and exceed the recommended value of 0.75. Based on the comparison given in Figure 7, the bounding epistemic uncertainty value of 0.75 (natural log units) was recommended as input with the (Zhao et al., 2006) attenuation model for the MAT PSHA sensitivity analysis.

### **Seismic Hazard Sensitivity Assessment**

Given the input source model for MAT and the recommended 1 Hz spectral acceleration ground motion model and epistemic uncertainty a MAT PSHA sensitivity analysis was performed. The resulting 1 Hz hazard curve including the MAT results was compared to the previous hazard curve results for the STP 3 & 4 site.

Comparison of the resulting 1 Hz hazard curve was made to an early version of the total PSHA using the significant updated EPRI-SOG sources. Note that the early version of the total PSHA was sufficiently similar to the final version, presented here, for the purposes of the sensitivity study. At the 1 Hz ground motion acceleration corresponding to the  $10^{-4}$  hazard level of the total hazard curve (excluding MAT contribution), the MAT hazard curve was less than 1% of that given by the total "base" hazard curve as is shown in Figure 8. As the MAT hazard curve decreases faster than the total hazard curve with increasing ground motion, the relative MAT

hazard at the  $10^{-5}$  hazard level of the total hazard would be even less, leading to the conclusion stated in the response to FSAR COM 2.5S-1 that, "...the MAT contribution to the total is too small for further PSHA consideration."

No COLA revision is required as a result of this RAI response.

**References:**

- Ammon, C.J., Ji, C., Thio, H.-K., Robinson, D., Ni, S., Hjorleifsdottir, V., Kanamori, H., Lay, T., Das, S., Helmberger, D., Ichinose, G., Polet, J., and Wald, D., 2005, Rupture process of the 2004 Sumatra-Andaman Earthquake: *Science*, v. 308, p. 1133-1139.
- Atkinson, G.M. and D.M. Boore, 2003, Empirical Ground-Motion Relations for Subduction-Zone Earthquakes and Their Application to Cascadia and Other Regions," *Bull. Seism. Soc. Am.*, Vol. 93, No. 4, pp. 1703-1729.
- Atkinson, G.M. and D.M. Boore, 1997, Stochastic Point-Source Modeling of Ground Motions in the Cascadia Region," *Seism. Res. Letters*, Vol. 68, No. 1, pp. 74-85.
- Azua, B.M., and DeMets, C., 2002, Strong interseismic coupling, fault afterslip, and viscoelastic flow before and after the Oct. 9, 1995 Colima-Jalisco earthquake: Continuous GPS measurements from Colima, Mexico: *Geophys. Res. Lett.*, v. 29, p. 122.
- Bandy, W., Kostoglodov, V., Hurtado-Díaz, A., and Mena, M., 1999, Structure of the southern Jalisco subduction zone, Mexico, as inferred from gravity and seismicity: *Geofísica Internacional*, v. 38, p. 127-136.
- Bird, P., 2003, An updated digital model of plate boundaries: *Geochemistry, Geophysics, Geosystems*, v. 4, p. 1027
- Bird, P., and Kagan, Y.Y., 2004, Plate-Tectonic Analysis of Shallow Seismicity: Apparent Boundary Width, Beta, Corner Magnitude, Coupled Lithosphere Thickness, and Coupling in Seven Tectonic Settings: *Bull. Seis. Soc. Am.*, v. 94, p. 2380-2399.
- Budnitz, R.J., Apostolakis, G., Boore, D.M., Cluff, L.S., Coppersmith, K.J., Cornell, C.A., and Morris, P.A., 1997, Recommendations for Probabilistic Seismic Hazard Analysis: Guidance on Uncertainty and Use of Experts: Washington, D.C., US Nuclear Regulatory Commission, NUREG/CR-6372, p. 278. EPRI (2004). CEUS Ground Motion Report, EPRI, Palo Alto, CA, Technical Report 1003647, 2003.
- Byrne, D.E., Davis, D.M., and Sykes, L.R., 1988, Loci and Maximum Size of Thrust Earthquakes and the Mechanics of the Shallow Region of Subduction Zones: *Tectonics*, v. 7, p. 833-857.
- Currie, C.A., Hyndman, R., Wang, K., and Kostoglodov, V., 2002, Thermal models of the Mexico subduction zone: Implications for the megathrust seismogenic zone: *J. Geophys. Res.*, v. 107, p. 2370.
- DeMets, C., Gordon, R.G., Argus, D.F., and Stein, S., 1994, Effect of recent revisions to the geomagnetic reversal timescale on estimates of current plate motions: *Geophys. Res. Lett.*, v. 21, p. 2191-2194.

- DeMets, C., and Traylen, S., 2000, Motion of the Rivera plate since 10 Ma relative to the Pacific and North American plates and the mantle: *Tectonophysics*, v. 318, p. 119-159.
- DeMets, C., and Wilson, D.S., 1997, Relative motions of the Pacific, Rivera, North America, and Cocos plates since 0.78: *J. Geophys. Res.*, v. 102, p. 2789-2806.
- Frohlich, C., and Wetzell, L.R., 2007, Comparison of seismic moment release rates along different types of plate boundaries: *Geophys. J. Int.*, v. 171, p. 909-920.
- Gregor, N.J., Silva, W., Wong, I., and Youngs, R., 2002, Ground-Motion Attenuation Relationships for Cascadia Subduction Zone Megathrust Earthquakes Based on Stochastic Finite-Fault Model: *Bull. Seis. Soc. Am.*, v. 92, p. 1923-1932.
- Hyndman, R.D., and Wang, K., 1993, Thermal constraints on the zone of major thrust failure, The Cascadia subduction zone: *J. Geophys. Res.*, v. 98, p. 2039-2060.
- Hyndman, R.D., Wang, K., and Yamano, M., 1995, Thermal constraints on the seismogenic portion of the southwestern Japan subduction thrust: *J. Geophys. Res.*, v. 100, p. 15,373-15,392.
- Iglesias, A., Cruz-Atienza, V.M., Shapiro, N.M., Singh, S.K., and Pacheco, J.F., 2001, Crustal structure of south-central Mexico estimated from the inversion of surface-wave dispersion curves using genetic and simulated annealing algorithms: *Geofisica Internacional*, v. 40, p. 181-190.
- Iglesias, A., Singh, S.K., Lowry, A.R., Santoyo, M., Kostoglodov, V., Larson, K.M., Franco-Sánchez, S.I., and Mikumo, T., 2004, The silent earthquake of 2002 in the Guerrero seismic gap, Mexico (Mw=7.4): inversion of slip on the plate interface and some implications: *Geofisica Internacional*, v. 43, p. 309-317.
- Kagan, Y.Y., 1999, Universality of the Seismic Moment-frequency Relation: *Pure and Applied Geophysics*, v. 155, p. 537-573.
- Kanno, T., A. Narita, N. Morikawa, H. Fujiwara and Y. Fukushima, 2006, A New Attenuation Relation for Strong Ground Motion in Japan Based on Recorded Data," *Bull. Seism. Soc. Am.*, Vol. 96, No. 3, pp. 879-897.
- Kostoglodov, V., Bandy, W., Dominguez, J., and Mena, M., 1996, Gravity and seismicity over the Guerrero seismic gap, Mexico: *Geophys. Res. Lett.*, v. 23, p. 3385-3388.
- Kostoglodov, V., Singh, S.K., Santiago, J.A., Franco, S.I., Larson, K., Lowry, A., and Bilham, R., 2003, A large silent earthquake in the Guerrero seismic gap, Mexico: *Geophys. Res. Lett.*, v. 30, p. 1807.
- Kostoglodov, V., Valenzuela, R.W., Gorbатов, A., Mimiaga, J., Franco, S.I., Alvarado, J.A., and Pelaez, R., 2001, Deformation in the Guerrero seismic gap, Mexico, from leveling observations: *J. Geodesy*, v. 75, p. 19-32.
- Larson, K.M., Kostoglodov, V., Miyazaki, S.i., and Santiago, J.A., 2007, The 2006 aseismic slow slip event in Guerrero, Mexico: New results from GPS: *Geophys. Res. Lett.*, v. 34, p. L13309.

- Larson, K.M., Lowry, A.R., Kostoglodov, V., Hutton, W., Sanchez, O., Hudnut, K., and Suarez, G., 2004, Crustal deformation measurements in Guerrero, Mexico: *J. Geophys. Res.*, v. 109, p. B04409.
- Lay, T., Kanamori, H., Ammon, C.J., Nettles, M., Ward, S.N., Aster, R.C., Beck, S.L., Bilek, S.L., Brudzinski, M.R., Butler, R., DeShon, H.R., Ekstrom, G., Satake, K., and Sipkin, S., 2005, The great Sumatra-Andaman Earthquake of 26 December 2004: *Science*, v. 308, p. 1127-1133.
- Manea, V., Manea, M., Kostoglodov, V., and Sewell, G., 2006, Intraslab seismicity and thermal stress in the subducted Cocos plate beneath central Mexico: *Tectonophysics*, v. 420, p. 389-408.
- Mann, P., Rogers, R., and Gahagan, L., 2006, Overview of plate tectonic history and its unsolved tectonic problem, in Bundschuh, J., and Alvarado, G.E., eds., *Central America: Geology, Resources and Hazards - 2 Volume Set (Hardcover)*: Netherlands, Balkema Publishers, p. 205-241.
- McCaffrey, R., 1993, On the Role of the Upper Plate in Great Subduction Zone Earthquakes: *J. Geophys. Res.*, v. 98, p. 11,953-11,966.
- McCaffrey, R., 2008, Global frequency of magnitude 9 earthquakes: *Geology*, v. 36, p. 263-266.
- McGuire, R.K., 2004, *Seismic Hazard and Risk Analysis*: Oakland, CA, Earthquake Engineering Research Institute.
- Megawati, K., T.C. Pan, and K. Koketsu, 2005, Response Spectral Attenuation Relationships for Sumatran-Subduction Earthquakes and the Seismic Hazard Implications to Singapore and Kuala Lumpur," *Soil Dynamics and Earthquake Engineering*, Vol. 25, pp. 11-25.
- Moore, J.C., and Saffer, D., 2001, Updip Limit of the Seismogenic Zone Beneath the Accretionary Prism of Southwest Japan: An Effect of Diagenetic to Low-Grade Metamorphic Processes and Increasing Effective Stress: *Geology*, v. 29, p. 183-186.
- Núñez-Cornú, F.J., Marta, R.L., P., F.A.N., Reyes-Dávila, G., and Suárez-Plascencia, C., 2002, Characteristics of seismicity in the coast and north of Jalisco Block, Mexico: *Phys. Earth Plan. Int.*, v. 132, p. 141-155.
- Oleskevich, D.A., Hyndman, R.D., and Wang, K., 1999, The updip and downdip limits to great subduction earthquakes: Thermal and structural models of Cascadia, south Alaska, SW Japan, and Chile: *J. Geophys. Res.*, v. 104, p. 14,965-14,991.
- Pacheco, J.F., Sykes, L.R., and Scholz, C.H., 1993, Nature of seismic coupling along simple plate boundaries of the subduction type: *J. Geophys. Res.*, v. 98, p. 14,133-14,159.
- Pan, T.C., K. Megawati, and C. L. Lim, 2007, Seismic Shaking in Singapore Deu to Past Sumatran Earthquakes," *Journal of Earthquake and Tsunami*, Vol. 1, No. 1, pp. 49-70.
- Pardo, M., and Suarez, G., 1995, Shape of the subducted Rivera and Cocos plates in southern Mexico: Seismic and tectonic implications: *J. Geophys. Res.*, v. 100, p. 12,357-12,373.
- Santoyo, M.A., Singh, S.K., Mikumo, T., and Ordaz, M., 2005, Space-Time Clustering of Large Thrust Earthquakes along the Mexican Subduction Zone: An Evidence of Source Stress Interaction: *Bull. Seis. Soc. Am.*, v. 95, p. 1856-1864.

- Tichelaar, B.W., and Ruff, L.J., 1993, Depth of seismic coupling along subduction zones: *J. Geophys. Res.*, v. 98, p. 2017-2037.
- Wells, D.L., and Coppersmith, K.J., 1994, New empirical relationships among magnitude, rupture length, rupture width, rupture area, and surface displacement: *Bulletin of the Seismological Society of America*, v. 84, p. 974-1002.
- Yoshioka, S., Mikumo, T., Kostoglodov, V., Larson, K.M., Lowry, A.R., and Singh, S.K., 2004, Interplate coupling and a recent aseismic slow slip event in the Guerrero seismic gap of the Mexican subduction zone, as deduced from GPS data inversion using a Bayesian information criterion: *Phys. Ear. Plan. Int.*, v. 146, p. 513-530.
- Youngs, R.R., S.J. Chiou, W.J. Silva, and J.R. Humphrey, 1997, Strong Ground Motion Attenuation Relationships for Subduction Zone Earthquakes," *Seism. Res. Letters*, Vol. 68, No. 1, pp. 58-73.
- Zhao, J.X., J. Zhang, A. Asano, Y. Ohno, T. Oouchi, T. Takahashi, H. Ogawa, K. Irikura, H.K. Thio, P. G. Sommerville, Ya. Fukushima, and Yo. Fukushima, 2006, Attenuation Relations of Strong Ground Motion in Japan Using Site Classification Based on Predominant Period, *Bull. Seism. Soc. Am.*, Vol. 96, No. 3, pp. 898-913.

**Table 1.** Parameters considered in the final source model. NA for the multiple segment fault source implies values should be taken from the individual component segments.

Source	Fault Trace	Fault Dip	Depth to Top of Seismogenic Rupture (km)	Depth to Bottom of Seismogenic Rupture (km)	Effective Slip Rate with Weights (mm/yr)	Slip Direction (degrees counterclockwise from north)	Mmax with Weights ( $M_w$ )
Jalisco-Rivera	(-106.89°, 21.80°) (-105.25°, 18.76°)	18.2°	6.6	38.5	5.76 [0.2] 9.60 [0.5] 13.43 [0.2] 17.27 [0.1]	209.81°	8.0 [0.2] 8.3 [0.6] 8.6 [0.2]
Michoacan	(-105.25°, 18.76°) (-100.87°, 16.64°)	17.5°	6.0	40.2	14.90 [0.2] 24.84 [0.5] 34.78 [0.2] 44.71 [0.1]	215.52°	8.1 [0.2] 8.4 [0.6] 8.7 [0.2]
Guerrero-Oaxaca	(-100.87°, 16.64°) (-97.69°, 15.51°)	11.9°	6.0	37.7	17.77 [0.2] 29.62 [0.5] 41.47 [0.2] 53.32 [0.1]	214.64°	7.9 [0.2] 8.3 [0.6] 8.7 [0.2]
Chiapas	(-97.69°, 15.51°) (-95.21°, 14.94°)	15.0°	8.8	38.5	19.73 [0.2] 32.89 [0.5] 46.04 [0.2] 59.19 [0.1]	213.59°	7.9 [0.2] 8.2 [0.6] 8.5 [0.2]
Michoacan to Chiapas	(-105.25°, 18.76°) (-100.87°, 16.64°) (-97.69°, 15.51°) (-95.21°, 14.94°)	NA	NA	NA	16.95 [0.2] 28.26 [0.5] 39.57 [0.2] 50.87 [0.1]	214.80°	8.6 [0.4] 8.85 [0.4] 9.1 [0.2]

**Table 2.** Models of single-segment vs. multi-segment rupture for the Michoacan to Chiapas rupture scenario.

Model	Single-Segment Rupture Frequency	Multi-Segment Rupture Frequency	Weight
Model 1	0.83	0.17	0.475
Model 2	0.9	0.1	0.475
Model 3	0.5	0.5	0.05

**Table 3.** Published attenuation models considered along with the defined site condition, magnitude and distance range applicability and type of data.

<i>Interface Subduction Zone Earthquakes</i>				
Model	Site Condition	Magnitude Range	Distance Range (km)	Data Type
Pan et al. (2007)	Crust (Vs=3.4km/sec)	5.0 – 9.0	300 – 1,200	Finite Fault Simulations
Megawati et al. (2005)	Hard Rock	4.5 – 8.0	150 – 1,500	Point Source Simulations
Youngs et al. (1997)	Rock	M > 5.0	10 – 500	Empirical Data
Atkinson and Boore (2003)	NEHRP B (Vs~1100m/sec)	M > 5.5	10 – 300	Empirical Data
Atkinson and Boore (1997)	Rock (Vs=1.5km/sec)	4.0 – 8.25	10 – 400	Point Source Simulations
Zhao et al. (2006)	Hard Rock (Vs=2.0km/sec)	5.0 – 8.3	<1 – 300	Empirical Data
Kanno et al. (2006)	Hard Rock (Vs=2.8km/sec)	5.5 – 8.3	1 – 400	Empirical Data

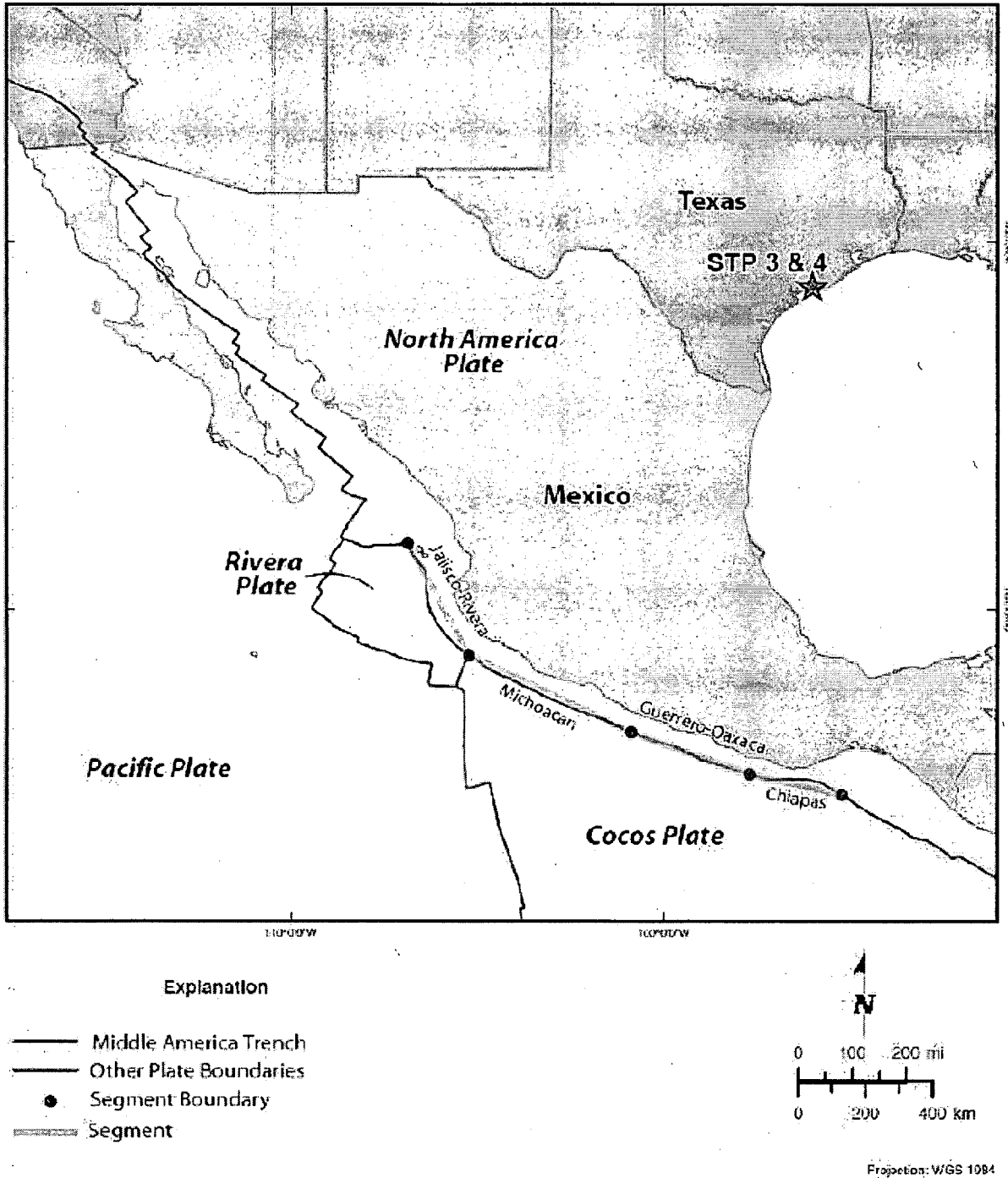


**Figure 1.** Rupture segments considered in the source model.

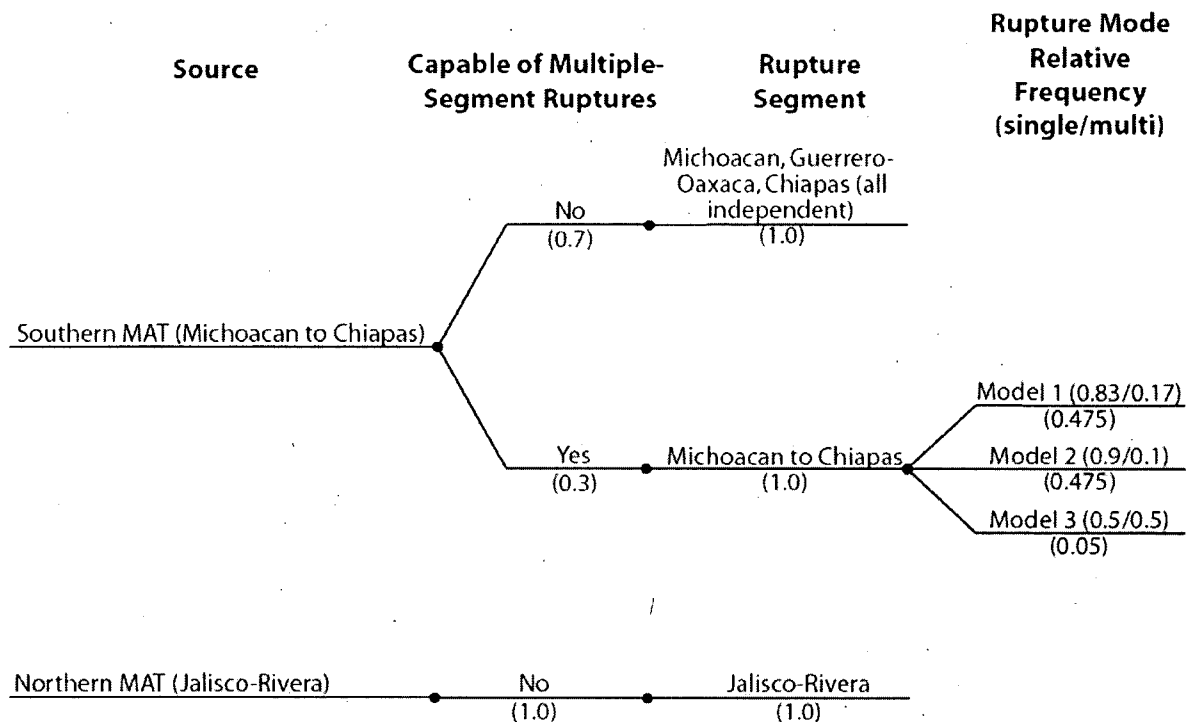


**Figure 2.** Logic tree of rupture scenarios for MAT sources.

**T=1.0sec Spectral Attenuation, M=6.5, Median**

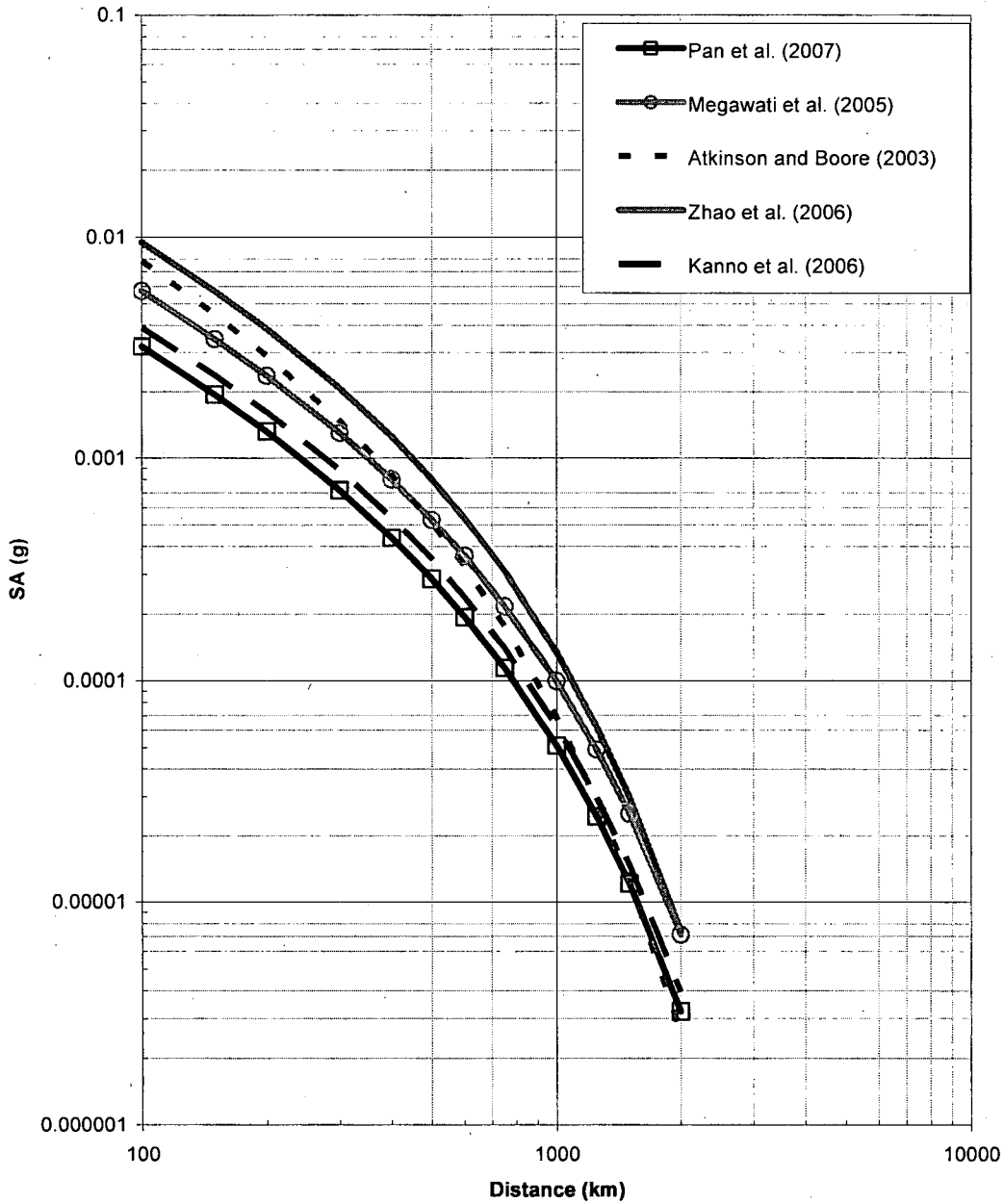


**Figure 3.** Comparison of median 1.0 sec attenuation curves for a magnitude 6.5 interface earthquake at distances between 100 and 2,000 km.

T=1.0sec Spectral Attenuation, M=7.5, Median

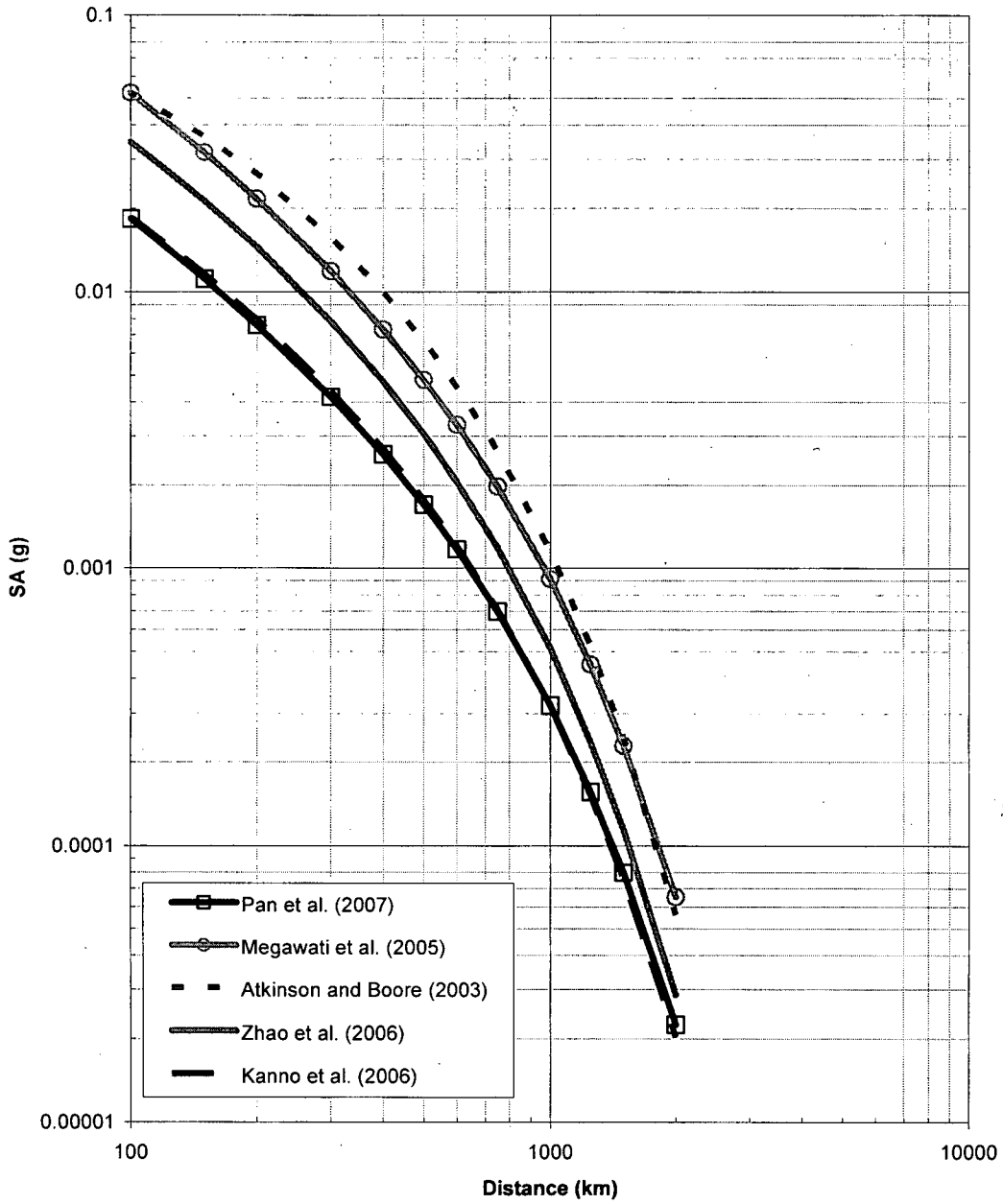
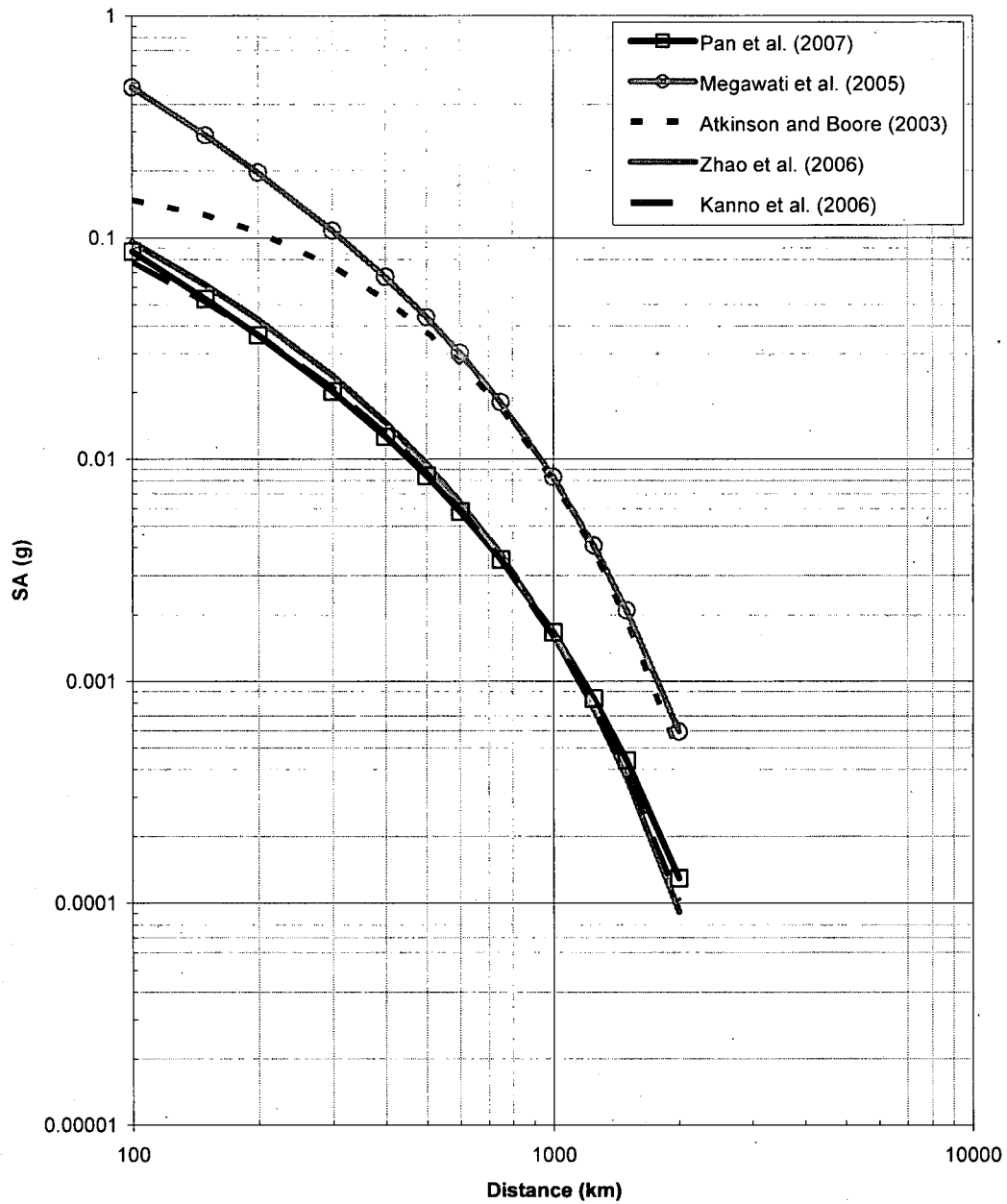


Figure 4. Comparison of median 1.0 sec attenuation curves for a magnitude 7.5 interface earthquake at distances between 100 and 2,000 km.

**T=1.0sec Spectral Attenuation, M=8.5, Median**



**Figure 5.** Comparison of median 1.0 sec attenuation curves for a magnitude 8.5 interface earthquake at distances between 100 and 2,000 km.

T=1.0sec Sigma

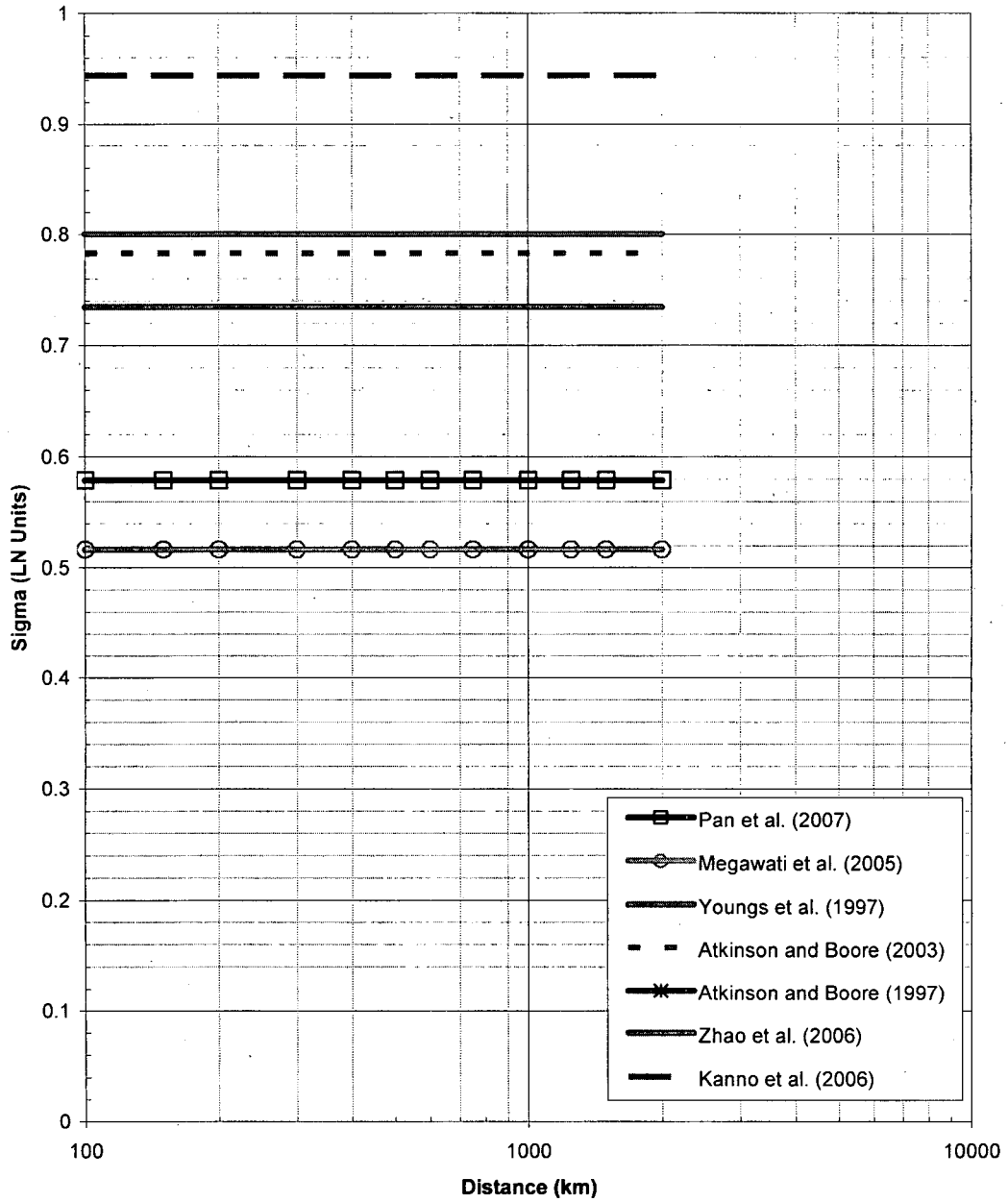
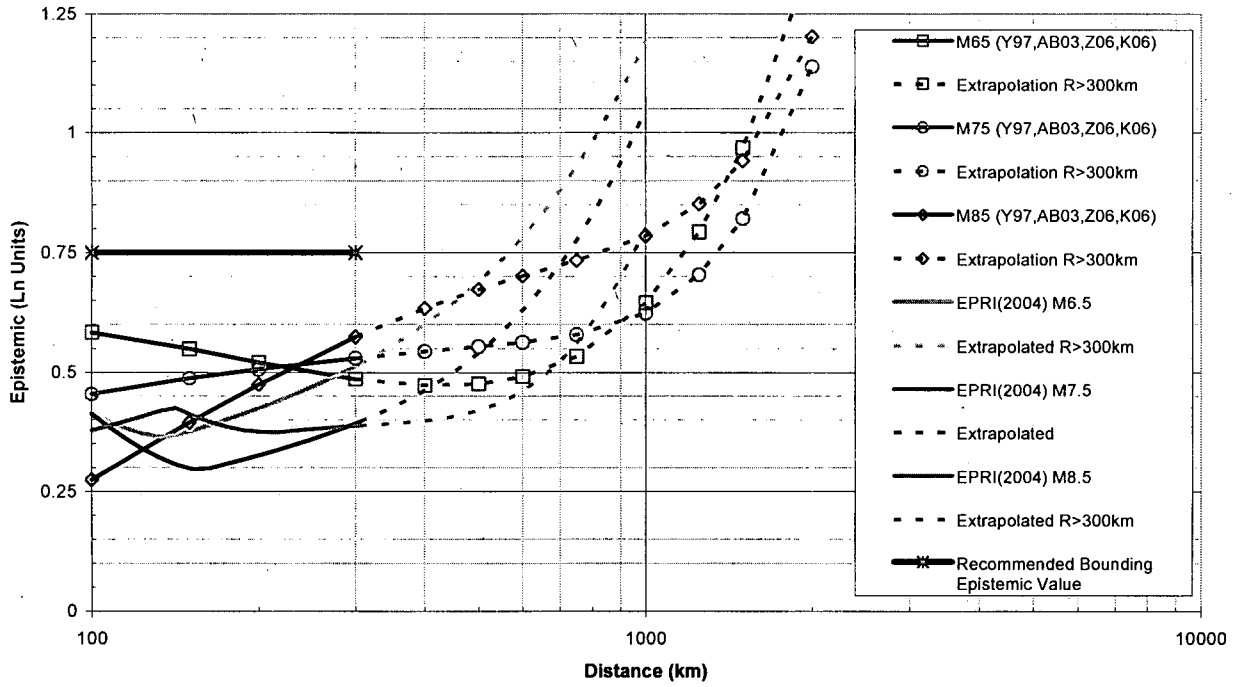
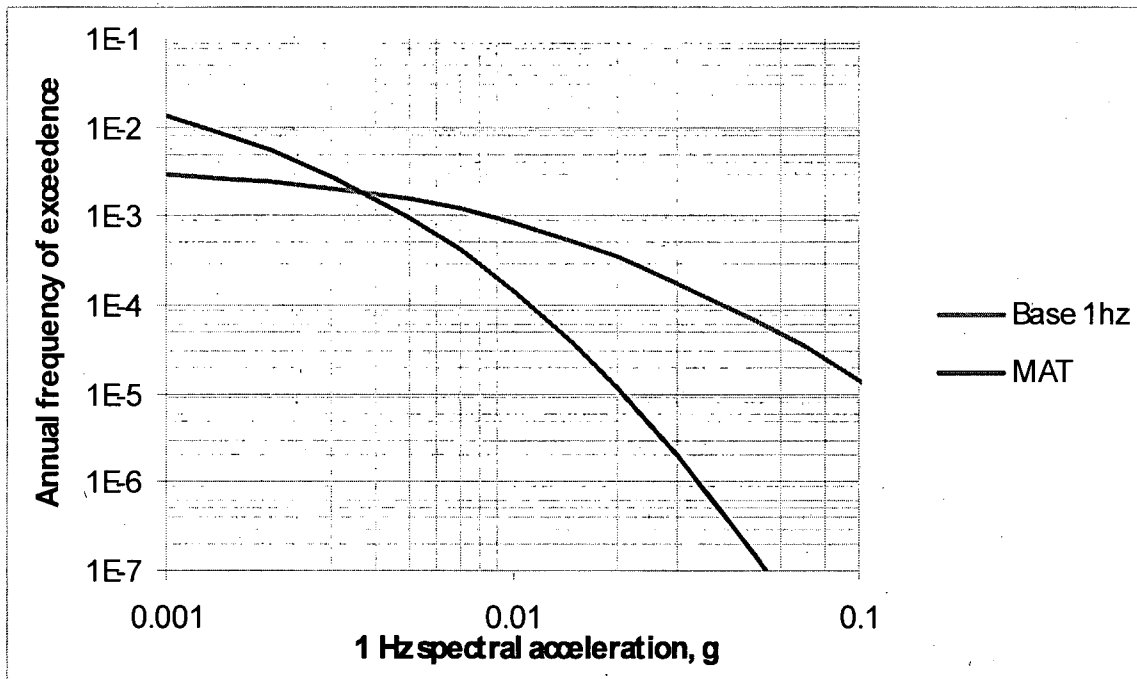


Figure 6. Comparison of 1.0 sec sigma values for interface earthquakes at distances between 100 and 2,000 km.

Epistemic Uncertainty



**Figure 7.** Comparison of 1.0 sec epistemic uncertainty values for magnitude 6.5, 7.5, and 8.5 from suite of empirically based subduction attenuation models and EPRI (2004) ground motion models. Recommended value of 0.75 is also plotted.



**Figure 8.** Mean 1 Hz hard rock hazard curves from base-rock calculation and current mid-America trench calculation.

**RAI 02.05.01-18****Question:**

In response to RAI 2.5.1-15, you described paleoseismic investigations of over 15 miles along the Colorado River within the STP site vicinity. Please provide information on the level of detail for these investigations, for instance (1) what were the site conditions, (2) what was the quality of the cutbank exposures, (3) were the sedimentary conditions appropriate for liquefaction to occur. Did you investigate smaller streams and tributaries along the Colorado River? Please provide the information that is specific to the paleoseismic portion of the field investigation.

**Response:**

As described in the response to RAI 02.05.01-15, the banks of the Colorado River within the greater site area (see FSAR Figure 2.5S.1-44 for the track of investigation) were examined by boat for the presence or absence of liquefaction features such as sand boils and sand dikes as part of a larger paleoliquefaction investigation.

Riverbank exposures on both sides of the Colorado River were relatively continuous at the time of the field reconnaissance. Recent flooding and associated higher flow rates had removed vegetation and produced fresh river-cut, near-vertical banks several meters high in many places. Because of the recent erosion, the riverbanks generally were well exposed with the exception of some areas with active slumping, man-made bank reinforcement, and undisturbed vegetation.

The riverbank exposures generally consisted of subhorizontal layers of interbedded silts and silty sand, with subordinate layers of coarser material including medium to fine-grained sand. These sandy layers likely correspond to point bar and channel bar deposits associated with well-developed channelbelts along the Colorado River. The sediments exposed in the riverbanks were sufficiently coarse and had low enough fines content to allow for liquefaction to occur during strong ground shaking. In addition, seepage and springs were observed in several locations along the banks indicating that shallow groundwater conditions necessary for liquefaction also were present.

Exposures were investigated for evidence of sand boils and other cross-cutting relationships typical of sub-surface liquefaction. The laterally continuous, layered stratigraphy was well-suited for identification of the presence or absence of paleo-liquefaction features. No features consistent with liquefaction at depth or near the surface were observed to truncate or cross-cut the laterally continuous, sub-horizontal stratigraphic boundaries between exposed layers indicating an absence of liquefaction.

Exposures also were investigated for the presence of relict lateral spreads, particularly within exposures of buried stream channels distinguished by tabular sand bodies and internal cross-beds. Several major slumps were observed along the Colorado River but these features were associated with recent, wholesale failure of the riverbanks based on the presence of fresh looking

margins and translocated vegetation within the headscarp areas of the failures. As such, these features are likely the result of lateral erosion and not strong ground shaking.

Smaller streams and tributaries along the Colorado River within the site vicinity were heavily vegetated and/or inaccessible by boat. The absence of observable outcrops and difficult access precluded examination of many of these secondary waterways during field investigation. However, several streams in the site vicinity were investigated by vehicle and foot access. Where exposures were visible, no evidence for liquefaction was found.

To provide further details within the FSAR with respect to the paleoliquefaction investigation, the text of Subsection 2.5S.1.2.6.4 will be replaced with the following:

#### **2.5S.1.2.6.4 Prior Earthquake Effects**

Studies of the STP 1 and 2 excavation and available outcrops examined during the STP 3 & 4 investigations have not indicated any evidence for prior earthquake activity that affected Pleistocene deposits.

Studies of the STP 1 and 2 excavation did not indicate any evidence for prior earthquake activity that affected Pleistocene deposits (e.g., paleoliquefaction and lateral spreading). As part of the STP 3 & 4 COLA, additional investigations were conducted to identify the presence or absence of paleoliquefaction features within the site region.

As described in Sections 2.5S.1 and 2.5S.2, an extensive review of published literature, government agency reports, and other materials was conducted for the STP 3 & 4 COLA. One focus of this review was the identification of any reported liquefaction features within the site region. This review of available literature (e.g., References 2.5S.1-49, 2.5S.1-50, 2.5S.1-YYY, and 2.5S.1-136) discovered no reported liquefaction features within the site region. The lack of any previously reported liquefaction features, as well as the absence of any moderate to large earthquakes within the site region within the historical record (see discussion in Section 2.5S.2) (e.g., References 2.5S.1-XXX, 2.5S.1-113, and 2.5S.1-115), suggest that the probability of liquefaction features present within the site region is small.

Despite the small likelihood of any liquefaction features existing within the site vicinity, investigations were carried out for the STP 3 & 4 COLA to identify the presence or absence of paleoseismic features within the greater site area. These investigations include the analysis of stereo-paired aerial photography and field reconnaissance. Analysis of the aerial photography focused on identifying any evidence of liquefaction (e.g., tonal variations from sand ejected during liquefaction, filling of contemporary fissures, and stream bank failure). All potentially anomalous geomorphic features identified in the aerial photos were further investigated (see Figures 2.5S.1-44 and 2.5S.1-45), and none of these features provided evidence of liquefaction.

During geologic field reconnaissance within the greater site area, exposures of Quaternary sediments were investigated for the presence of liquefaction features. The best exposures of sediments within the site vicinity were of the Pleistocene Beaumont Formation and associated younger deposits (Reference 2.5S.1-38) along the banks of the Colorado River. Over 15 miles of riverbank along the Colorado River were

investigated within the greater site vicinity for the presence of liquefaction features (see Figure 2.5S.1-44).

Riverbank exposures on both sides of the Colorado River were relatively continuous at the time of the field reconnaissance. Recent flooding and associated high stream flows had removed vegetation and produced fresh river-cut, near-vertical banks several meters high in many places. Because of the recent erosion, the riverbanks generally were well exposed with the exception of some areas with active slumping, man-made bank reinforcement, and undisturbed vegetation.

The riverbank exposures generally consisted of subhorizontal layers of interbedded silts and silty sand, with subordinate layers of coarser material including medium to fine-grained sand. These sandy layers likely correspond to point bar and channel bar deposits associated with well-developed channelbelts along the Colorado River. The sediments exposed in the riverbanks were sufficiently coarse and had low enough fines content to allow for liquefaction to occur during strong ground shaking. In addition, seepage and springs were observed in several locations along the banks indicating that the shallow groundwater conditions necessary for liquefaction also were present.

Exposures were investigated for evidence of sand boils and other cross-cutting relationships typical of sub-surface liquefaction. The laterally continuous, layered stratigraphy was well-suited for identification of the presence or absence of paleo-liquefaction features. No features consistent with liquefaction at depth or near the surface were observed to truncate or cross-cut the laterally continuous, sub-horizontal stratigraphic boundaries between exposed layers indicating an absence of liquefaction.

Exposures also were investigated for the presence of relict lateral spreads, particularly within exposures of buried stream channels distinguished by tabular sand bodies and internal cross-beds. Several major slumps were observed along the Colorado River but these features were associated with recent, wholesale failure of the riverbanks based on the presence of fresh looking margins and translocated vegetation within the headscarp areas of the failures. As such, these features are likely the result of lateral erosion and not strong ground shaking.

Smaller streams and tributaries along the Colorado River within the site vicinity were heavily vegetated and/or inaccessible by boat. The absence of observable outcrops and difficult access precluded examination of many of these secondary waterways during field investigation. However, several streams in the site vicinity were investigated by vehicle and foot access. Where exposures were visible, no evidence for liquefaction was found.

In summary, the investigations undertaken for the STP 3 & 4 COLA uncovered no evidence of prehistoric strong ground shaking (e.g. liquefaction, lateral spreading).

The following new references will be added to Subsection 2.5S.1.3:

2.5S.1-XXX	Davis, D.M., Pennington, W., and Carlson, S., 1985, Historical seismicity of the state of Texas: a summary. Gulf Coast Association of Geological Societies Transactions, v. 35, p. 39-44.
2.5S.1-YYY	Wheeler, R.L., 2006, Quaternary tectonic faulting in the eastern United States: Engineering Geology, v. 82, p. 165-186.

References:

- 2.5S.1-38 Blum, M.D., and Aslan, A., 2006, Signatures of climate vs. sea-level change within incised valley-fill successions: Quaternary examples from the Texas Gulf Coast: Sedimentary Geology, v. 190, p. 177-211.
- 2.5S.1-49 Crone, A.J., and Wheeler, R.L., 2000, Data for Quaternary faults, liquefaction features, and possible tectonic features in the Central and Eastern United States, east of the Rocky Mountain front, U.S. Geological Survey Open-File Report 00-260, p. 342.
- 2.5S.1-50 Wheeler, R.L., 2005, Known or Suggested Quaternary Tectonic Faulting, Central and Eastern United States—New and Updated Assessments for 2005, U.S. Geological Survey Open-File Report 2005-1336, p. 40.
- 2.5S.1-113 Davis, S.D., Pennington, W.D., and Carlson, S.M., 1989, A compendium of earthquake activity in Texas, University of Texas at Austin, Bureau of Economic Geology, Geological Circular 89-3.
- 2.5S.1-115 Frohlich, C., and Davis, S.D., 2002, Texas Earthquakes: Austin, University of Texas Press, 275 p.
- 2.5S.1-136 Wheeler, R.L., and Crone, A.J., 2001, Known and suggested Quaternary faulting in the midcontinent United States: Engineering Geology, v. 62, p. 51-78.

**RAI 02.05.02-19****Question:**

FSAR Section 2.5S.1.2.4.3, states in the “Summary” subsection that fault GMP (FSAR Reference 2.5S.1-124) extends beneath the cooling reservoir and is the closest growth fault to STP Units 3 and 4, with a surface projection approximately 1.4 miles from Units 3 and 4. Since this is the closest growth fault feature to the STP site, and due to the fact that it was not previously characterized in the FSAR for Units 1 and 2, please describe this fault more thoroughly, including whether any additional investigations were performed, and if so what the results were. If additional investigations were not performed, please explain why, given the proximity of the fault to the site.

**Response:**

Growth fault GMP is represented as a short, north-northwest-trending projection (e.g., see Figure 2.5S.1-45) within the STP 3 & 4 FSAR. This projection of GMP suggests that, at depth, the growth fault GMP may trend north towards the STP 3 & 4 site. However, this perceived trend based on the surface projection does not represent the trend of the growth fault at depth. Based on an analysis of Geomap structural contour maps summarized below, the trend of GMP at depth illustrates that the growth fault trends to the west, subparallel to the surface projection of growth fault GMO and not to the north towards the STP 3 & 4 site. The contrast in trend of the surface projection to the trace of the fault at depth is due to limitations associated with developing the growth fault surface projections. Therefore, it was determined that growth fault GMP does not pose a surface deformation hazard for the site. This conclusion is supported by the seismic reflection studies that were conducted as part of the investigations for STP Units 1 & 2 that demonstrated no growth faults project to the surface at the STP 3 & 4 site.

As shown in Figures 2.5S.1-5 and 2.5S.1-42 and discussed in Subsection 2.5S.1.1.4.4.2, growth faults trend roughly parallel to the coastline at both regional and local scales. The trend of growth fault GMP’s surface projection significantly deviates from this trend (see Figure 2.5S.1-42), but this deviation is an artifact of the data and methodology used to develop the projection and does not reflect the true trend of the growth fault. As described within FSAR Subsection 2.5S.1.2.4.2.2.1 and in response to RAI question 02.05.01-7, the growth fault projections, including that of GMP, were generated from structural contour maps published by Geomap Company (Reference 2.5S.1-124). These maps present structural contours of two separate horizons and the locations of growth faults at those horizons. As described in response to RAI questions 02.05.01-13 and 02.05.01-7, the locations of the growth faults and the depths of the horizons are largely based on interpretation of well-log data. The projection of GMP presented in the STP 3 & 4 COLA was developed by:

- Identifying the trace of GMP in both horizons;
- Determining the elevation of discrete points along the trace of both horizons by noting where the trace crosses a structural elevation contour;

- Using the discrete elevations in both horizons to develop projected locations of GMP at the surface; and
- Drawing a smooth trace through the individually projected points.

Within the Geomap data, growth fault GMP is mapped as a short splay of the extensively mapped growth fault GMO that initiates at approximately the same longitude as the STP 3 & 4 site. Within the upper horizon of the Geomap data, GMP is represented as a splay to the north of GMO that trends westward subparallel to GMO for a total distance of approximately 3 miles, well beyond the longitude of the STP 3 & 4 site. Within the lower horizon of the Geomap data, GMP is only identified as an approximately 1 mile long splay, initiating at the same location and trending predominately northwest. The western ends of the GMP traces at depth correlate with the region of the Geomap data with poor well control, and it is likely that the lack of further western continuations in both horizons is due to a lack of data (see discussion in response to RAI question 02.05.01-13). However, given the strong regional and local trend of growth faults, if GMP does extend beyond the extent mapped within the Geomap data, it is most likely that GMP continues subparallel to GMO.

As described above, the geometry of the GMP surface projection depends on the location of the fault within both Geomap horizons. Also as described above, GMP within the lower horizon is shorter than within the upper horizon, so the extent of GMP within the lower horizon dictates the extent of the GMP surface projection. Within the lower horizon GMP is only mapped where it trends northwest and does not extend to where the trend bends westward following GMO. Therefore, the surface projection of GMP only reflects this northwesterly trend and does not reflect the full behavior of GMP evident in the upper horizon data where the fault curves westward and follows the trend of GMO well beyond the longitude of the STP 3 & 4 site. These basic observations concerning GMP, combined with the conclusions of the STP 1 & 2 UFSAR that no growth faults project to the surface within the STP 3 & 4 site, demonstrate that growth fault GMP does not present a hazard for the STP 3 & 4 site. Therefore, no additional investigations of GMP were conducted besides those discussed in the STP 3 & 4 COLA and clarified in previous responses to RAIs.

Note that a typographical error in the COLA describes growth fault GMP as trending to the north-northeast (Subsection 2.5S.1.2.4.3) and should read north-northwest. The first sentence of the second paragraph of Subsection 2.5S.1.2.4.3 will be replaced with the following to correct the typographical error:

Among the growth faults in the site area not recognized in the UFSAR for STP 1 & 2, fault GMP (Reference 2.5S.1-124), which trends north-northwest and is located beneath the southern part of the cooling reservoir, is the structure with the closest surface projection to STP 3 & 4 (approximately 1.4 mile) (Figure 2.5S.1-43 [References 2.5S.1-7, 2.5S.1-124, and 2.5S.1-151]).

Among the growth faults in the site area not recognized in the UFSAR for STP 1 & 2, fault GMP (Reference 2.5S.1-124), which trends north-northwest and is located beneath the southern part of the cooling reservoir, is the structure with the closest surface projection to

STP 3 & 4 (approximately 1.4 mile) (Figure 2.5S.1-43 [References 2.5S.1-7, 2.5S.1-124, and 2.5S.1-151]).

References:

- 2.5S.1-124 "Upper Texas Gulf Coast Mapping Service maps 327 and 328," Geomap, 2007. Licensed from Geomap Company to William Lettis and Associates, Inc. from February 1, 2007 to January 31, 2008.

**RAI 02.05.02-20****Question:**

In response to RAIs 2.5.1-13 and 2.5.1-14, you stated that the growth fault STP12I/GMO does not trend eastward into the cooling reservoir and this information appears to be based largely on results from topographic profile STP L4. In addition, you investigated the area south of the reservoir for associated features. In revised FSAR Figure 2.5S.1 45, provided in response to RAI 2.5.1-13, there are features (within the cooling reservoir) that represent slope breaks and vegetation lineaments along a northeast trend and along strike with growth fault GMO/STP12I (as it is projected west of the cooling reservoir). These features appear to be continuous toward the center of the cooling reservoir. FSAR Section 2.5S.1.2.4.2.2.1 states that potential uncertainty associated with projecting growth fault locations may vary as much as several miles as well as along strike and “between different faults”. In light of this, the slope breaks and linear vegetation features shown on revised FSAR Figure 2.5S.1-45 may represent a northeast extension of growth fault GMO/STP12I at the surface, placing the fault within the cooling reservoir and closer to STP Units 3 and 4. Please discuss these linear features.

**Response:**

With respect to growth fault GMO, the response to RAI 02.05.01-13 states that “... post-Beaumont surface deformation associated with the growth fault does not trend eastward into the cooling reservoir.” As described in FSAR Section 2.5S.1.2.4.2, this conclusion is based on the results of topographic surveys across growth fault GMO that demonstrated evidence for surface deformation along three topographic surveys west of the reservoir but not along a fourth survey conducted adjacent to the reservoir. The present RAI question is essentially addressing whether surface deformation related to growth fault GMO is present beneath the reservoir given the observations stated in the RAI that: (1) the surface projection of growth fault GMO is uncertain, and (2) lineaments identified from preconstruction aerial photographs occur along the trend of growth fault GMO within the reservoir. As part of the STP 3 & 4 investigations, it was determined that these lineaments were not related to surface deformation from growth fault GMO because: (1) given the estimated uncertainty in the projection of GMO, it is unlikely that GMO would project to the location of the observed lineaments within the reservoir; and (2) the vast majority of the lineaments within the cooling reservoir are vegetation lineaments, not slope breaks.

As demonstrated by the spatial coincidence of the GMO surface projection and the monoclinial folding identified on the topographic profiles, surface deformation associated with GMO correlates closely with the GMO surface projection (see responses to RAIs 02.05.01-7 and 02.05.01-9). Based on this correlation, it is assumed that the surface projection of growth fault GMO accurately identifies the true updip projection of GMO west of the reservoir. Therefore, it is expected that within the cooling reservoir, the true updip projection of GMO should be within the expected uncertainty bounds of the GMO projection developed within the FSAR. The expected uncertainty bounds for the projection of GMO were presented in response to RAIs 02.05.01-7 and 02.05.01-9 (Letter ABR-AE-08000074, October 1, 2008), and, as Figure 18 of

RAI response 02.05.01-7 demonstrates, the projection of GMO, including its expected uncertainty, is well south of the lineaments within the cooling reservoir. Based on this observation, it is considered very unlikely that the lineaments within the reservoir are related to growth fault GMO.

The lineament analysis for STP 3 & 4 included examination of stereo pairs of various sets of aerial photographs taken before, during, and after construction of STP Units 1 and 2 to identify tonal lineaments and potentially anomalous geomorphic features. These features include closed depressions, vegetation lineaments, linear drainages, and subtle south-facing slope breaks (some of which are spatially associated with growth fault GMO). The identified lineaments were further investigated during aerial and field reconnaissance efforts to identify the causative source of the lineament. As a result of these investigations, many lineaments initially identified as slope breaks were reclassified as vegetation lineaments based on: (1) direct observation of the absence of discrete topographic variation on the land surface; and (2) association of the lineaments with cultural features (e.g., farm roads and drainage ditches) and changes in vegetation.

The vast majority of lineaments identified within the cooling reservoir were mapped as vegetation lineaments based on observations made from the aerial photographs. As shown in FSAR Figure 2.5S.1-45, only two relatively short potential slope-break lineaments were identified within the cooling reservoir. Because the reservoir now covers the land surface on which the lineaments were observed, these lineaments could not be further investigated during aerial and field reconnaissance, thus, preventing confirmation of their presence and origin. However, similar slope-break lineaments in the site area but outside of the cooling reservoir that were identified on pre-construction aerial photographs are commonly found to lack topographic expression. Upon field investigation, these lineaments that were originally identified as possible slope breaks were found to reflect localized vegetation patches that appear dark in the black and white photographs, similar to shadows often associated with slope breaks.

Even though the presence of these lineaments within the reservoir and their origin (e.g., growth fault activity, fluvial modifications, cultural feature) could not be independently verified, these lineaments were conservatively retained on the map. However, based on the location of the surface projection of GMO, the absence of a clear topographic signal of monoclinial folding adjacent to the reservoir, and the presence of only two potential slope-break lineaments identified within the cooling reservoir, it was concluded that the trend of lineaments extending to the northeast into the cooling reservoir likely does not reflect surface deformation related to growth fault GMO.

No COLA revision is required as a result of this RAI response.

**RAI 02.05.01-21****Question:**

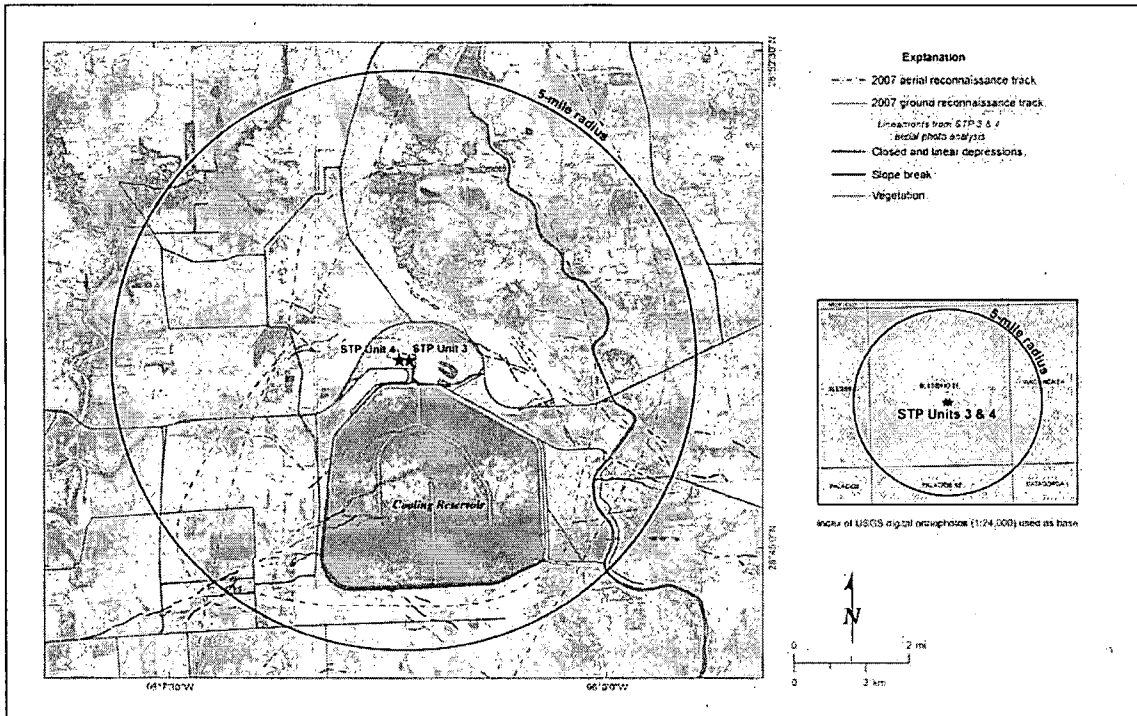
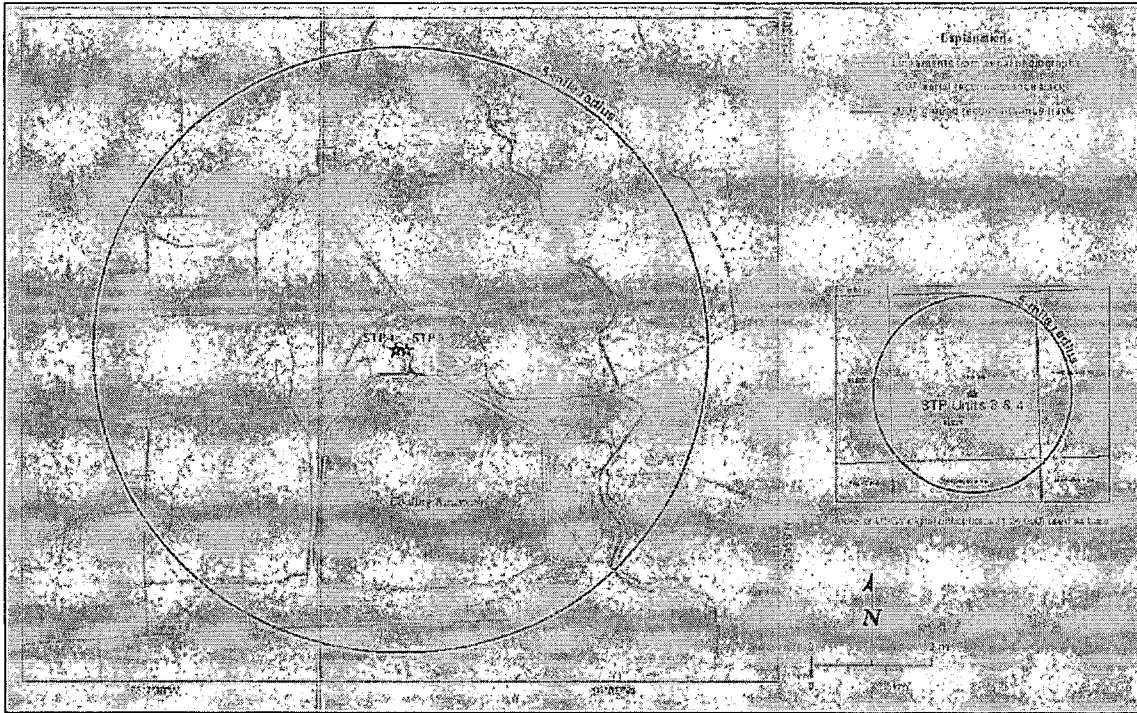
FSAR Sections 2.5S.1.1.4.4.5.4, 2.5S.1.2.4.2, 2.5S.1.2.4.3, and 2.5S.3.2.2 provide evaluations of growth faults and the potential for Quaternary growth faulting in the STP site vicinity. This data is based on investigations performed for STP Units 1 and 2 and more recently for STP Units 3 and 4. In order for the staff to perform an adequate evaluation of the potential for growth faulting within the 5-mile STP radius, and specifically within the 0.6-mile site radius, please provide the following:

- a.) FSAR figure 2.5S.1-44 suggests that it represents lineament data in addition to aerial reconnaissance and ground reconnaissance tracks. Please revise FSAR Figure 2.5S.1-43, 44, and 45 to include lineament data that is described in the "Explanation", or legend, so that the staff can adequately evaluate the extent of the growth fault investigations within the site area, or within the 5-mile site radius. In addition, please identify which linear features were identified in the investigations for STP Units 1 and 2 and which features were identified in the investigations for Units 3 and 4.
- b.) In FSAR Section 2.5S.3, only two growth faults were interpreted to approach within 5,000 ft of the ground surface and these two faults were mapped to within 800 ft and 1000 ft of the surface, respectively. However, in FSAR Section 2.5S.1 for Units 3 and 4, and in the UFSAR for STP Units 1 and 2, three faults were described that approach within 5,000 ft of the surface (faults A, I, and J) and one of those faults, growth fault A, was interpreted from reflection data to approach the limit of resolution, approximately 500 meters below the surface. Please resolve this information in the FSAR.
- c.) Please describe the resolution limits associated with the data used to interpret growth faulting, or lack of growth faulting within the upper 1000 meters, or within Quaternary units in the site area.

**Response:**

- a.) Revised FSAR Figures 2.5S.1-44 and 2.5S.1-45 were presented in the responses to RAIs 02.05.01-8 (Letter ABR-AE-08000054, July 16, 2008) and 02.05.01-13 (Letter ABR-AE-08000061, August 12, 2008). These revised figures included the location of lineaments identified from aerial photos as part of the STP 3 & 4 investigations. FSAR Figures 2.5S.1-44 and 2.5S.1-45 have been further revised in this RAI response to more clearly indicate within the explanations that the lineaments shown in the figures were identified as part of the STP 3 & 4 investigations. Lineaments identified during the STP Units 1 and 2 efforts are presented in the responses to RAIs 02.05.01-7 and 02.05.01-9 (Letter ABR-AE-08000074, October 1, 2008). FSAR Figure 2.5S.1-43 has not been modified in response to this RAI because that figure does not present and is not intended to present lineaments. The figure is intended to only show the location of growth fault surface projections.

Replace Figure 2.5S.1-44 with the revised version shown below:





- b.) The apparent discrepancy noted in the RAI question is related to a typographical error in the STP 3 & 4 FSAR. The affected sections of the FSAR will be modified as follows to correct the typographical error and to further clarify the noted discrepancy.

The first paragraph of FSAR Section 2.5S.3.2.2.1 will be replaced with the following:

As discussed in Subsection 2.5S.1.2.4.1.2.1, Subsection 2.5.1.2.5.3 of the STP 1 & 2 UFSAR (Reference 2.5S.3-1) documents the presence of 10 growth faults within the site area. These faults are confined to the Mesozoic and Cenozoic Gulf Coastal Plain stratigraphic section and do not extend into the underlying crystalline basement. Subsection 2.5.1.2.5.3 of the STP 1 & 2 UFSAR presents seismic reflection and borehole data that demonstrate 8 of the 10 growth faults in the site area are buried by 5000 ft. or more of undisturbed sediments that are Miocene in age or younger, indicating that there has been no movement on these 8 faults in the past 5 million years or longer. Two of these growth faults ("A" and "I"; Figure 2.5S.1-43) exhibit evidence for deformation younger than Miocene and can be traced on seismic reflection profiles to within 800 ft. to 1000 ft. or less of the ground surface. The closest approach of growth faults "A" and "I" to the STP site area is approximately 3.0 miles and 3.8 miles, respectively. Subsection 2.5.1.2.5.3 of the STP 1 & 2 UFSAR notes that this depth range is the effective limit of resolution of the seismic reflection data, and thus the reflection data can not be used to assess whether the faults approach closer to the surface than 800 ft. to 1000 ft. Based on field reconnaissance and inspection of a shallow excavation along the western margin of the main cooling water reservoir, Subsection 2.5.1.2.5.3 of the STP 1 & 2 UFSAR (Reference 2.5S.3-1) contains conclusions that there is no discrete displacement of the land surface, or of continuous stratigraphic contacts in the shallow subsurface, above the up-dip projections of growth faults "A" and "I."

As discussed in Subsection 2.5S.1.2.4.1.2.1, Subsection 2.5.1.2.5.3 of the STP 1 & 2 UFSAR (Reference 2.5S.3-1) documents the presence of 10 growth faults within the greater site area. These faults are confined to the Mesozoic and Cenozoic Gulf Coastal Plain stratigraphic section and do not extend into the underlying crystalline basement. Subsection 2.5.1.2.5.3 of the STP 1 & 2 UFSAR presents seismic reflection and borehole data that demonstrate 8 of the 10 growth faults are buried by 3900 ft. or more of undisturbed sediments that are at least Pliocene and probably Miocene in age or younger, indicating that there has been no movement on these 8 faults in the past approximately 3 million years or longer. Two of these growth faults ("A" and "I"; Figure 2.5S.1-43) exhibit evidence for Miocene to Pliocene or younger deformation and can be traced on seismic reflection profiles to within 900 ft. or less of the ground surface. The closest approach of growth faults "A" and "I" to the STP site is approximately 3.0 miles and 3.8 miles, respectively. Subsection 2.5.1.2.5.3 of the STP 1 & 2 UFSAR notes that this depth range is the effective limit of resolution of the seismic reflection data, and thus the reflection data cannot be used to assess whether the faults approach closer to the surface. Based on field reconnaissance and inspection of a shallow excavation along the western margin of the main cooling water reservoir, Subsection 2.5.1.2.5.3 of the STP 1 & 2 UFSAR (Reference 2.5S.3-1) contains conclusions that there is no discrete displacement of the land surface, or of continuous stratigraphic contacts in the shallow subsurface, above the up-dip projections of growth faults "A" and "I."

The first bullet in the second paragraph of FSAR Section 2.5S.3.4.1 will be replaced with the following:

~~Eight of the 10 growth faults are overlain by undeformed deposits of Miocene age or older. Based on these relations, the UFSAR concluded that these eight growth faults have not been active since Miocene time.~~

Eight of the 10 growth faults are overlain by undeformed deposits of at least Pliocene and probably Miocene age or older. Based on these relations, the UFSAR concluded that these eight growth faults have not been active since approximately Miocene time.

- c.) For the STP 3 & 4 site, the presence or absence of growth faults within Quaternary deposits and/or those deposits within 1000 meters of the surface was documented using two primary modes of observation: (1) subsurface observations (e.g., seismic reflection data) capable of identifying growth faults within the subsurface, and (2) surface observations (e.g., aerial photos analysis, ground reconnaissance, aerial reconnaissance, and topographic surveys) capable of identifying surface deformation associated with shallow growth faults. The use of each of these modes of observation with respect to the study of growth faults for STP 3 & 4 is described in detail in FSAR Section 2.5S.1.2.4 and in the responses to RAIs 02.05.01-7 through 02.05.01-14, 02.05.01-19, 02.05.01-20, and 02.05.03-1. The following discussion presents a summary of the resolution limits of these modes of observation for identifying the presence or absence of growth faulting.

#### Subsurface Observations

In general, growth faults identified at relatively shallow depths tend to sole into deeper growth fault systems. For example, within the STP site area most growth faults are from the Frio growth fault system and thus sole into Frio-age or older stratigraphic horizons (see discussion within FSAR Sections 2.5S.1.1.4.4.4.2 and 2.5S.1.2.4.2). Within the site area, these horizons are generally at considerable depth (i.e., 1000s of meters below the surface). As such, the ability to assess the absence of growth faults within the site area at shallow depths (100s of meters or less) can also depend on the ability to demonstrate the absence of growth faults extending upward from these greater depths.

As described in the STP 3 & 4 FSAR, the conclusions of the extensive seismic reflection study completed as part of the UFSAR for STP Units 1 and 2 were used to identify the location of growth faults within the STP 3 & 4 site area at depth and demonstrate the absence of growth faults that would project to within the STP 3 & 4 site. As stated in the response to RAI 02.05.01-7, the UFSAR for STP Units 1 and 2 and its supporting materials do not include an explicit discussion of the resolution of the seismic reflection data. Thus, no direct statement can be made about the resolution limits of the seismic reflection data used in the STP Units 1 and 2 efforts for identifying growth faults. However, indirect inferences of the resolution can be made.

Seismic reflection Line 2M (see response to RAI 02.05.01-7) provides some of the best constraints on the presence and absence of growth faults within the site area and beneath the site. Based on observations made of Fault I in Line 2M and discussed in the UFSAR for STP Units 1 and 2, it is known that at a minimum Line 2M is capable of resolving 40

ft of offset from growth faulting at a depth of 900 ft. Therefore, it is reasonable to assume that any fault with 40 ft or more of offset at 900 ft depth along Line 2M has been identified. At greater depths it is likely that a similar resolution exists, so it is reasonable to assume any fault with offsets of approximately 40 ft or more at depths greater than 900 ft along Line 2M was also identified as part of the STP Units 1 and 2 efforts.

Additional support for the absence of growth faults at shallow depths comes from the fact that growth faults tend to have greater offsets down-dip along their fault plane because the up-dip portions of the fault are younger and have experienced less slip. For example, a growth fault that formed during deposition of the Frio Formation may extend to the shallow subsurface, but the maximum offset across such faults is typically observed in the deeper Frio Formation and not the shallower and younger deposits. Fault I shows this behavior with approximately 40 ft of offset at a depth of 900 ft and approximately 500 ft of offset at a depth of 5000 ft (see RAI response 02.05.01-7). Therefore, growth faults with small offsets at shallow depth should be easier to identify at greater depths where they will have larger offsets. The fact that the STP Units 1 and 2 studies did not observe such faults at depth projecting to within the site footprint is strong, positive evidence for a lack of growth fault hazard at the STP 3 & 4 site.

#### Surface Observations

For the STP 3 & 4 site, the presence or absence of permanent ground deformation hazard within the site area due to growth faults also is documented through the presence or absence of surface deformation related to growth fault activity. As described in detail in FSAR Section 2.5S.1.2.4.2.2.2 and in the responses to RAIs 02.05.01-9, 02.05.01-10, and 02.05.01-12, surface deformation associated with growth fault activity is represented as broad, monoclinial folding and tilting of the ground surface. The observation and documentation of such folding suggests the presence of a surface-deforming growth fault, and the absence of such folding indicates the absence of a surface-deforming growth fault.

As described in detail in FSAR Section 2.5S.1.2.4.2, the only monoclinial surface folding related to growth faults within the site area was the folding associated with Fault I. The folding associated with Fault I was identified with aerial photo analysis and verified via field reconnaissance. Therefore, the question of resolution limits for identifying growth fault monoclinial folding is dependent on the methodology of identifying monoclinial folding with ground reconnaissance and analysis of aerial photography and because both of these methods are based on interpretation of qualitative observations there is no quantitative measure of resolution limits. However, the observation of folding associated with Fault I does provide a bounding estimate for the amplitude of folding and flexure that can be resolved. As described in FSAR Section 2.5S.1.2.4.2.2.2, the monoclinial folding associated with Fault I is characterized by an increase in surface slope of  $0.3^\circ$  to  $0.5^\circ$  across the fold resulting in a total structural relief of 1 to 6 ft. Accordingly, it is reasonable to assume that the air photo analysis and ground observations made as part of the STP 3 & 4 efforts should be capable of resolving the presence or absence of

monoclinal folds with a  $0.3^\circ$  change in the surface slope and/or a total structural relief of 1 ft.

The issue of the temporal persistence of such folding was addressed in the responses to RAIs 02.05.01-10 and 02.05.01-12. The general conclusion presented in those responses is that: (1) monoclinal folding occurring at any time since the deposition of the Beaumont surface should be presently observable, and (2) the absence of monoclinal folding indicates the absence of any growth fault related surface deformation since deposition of the Beaumont formation.

Commitment Number	Commitment Statement	Due Date
09-10843-1	RAI 02.05.02-19 includes changes to STP COLA Part 2, Tier 2, Subsection 2.5S.2.5, "Seismic Wave Transmission Characteristic of the Site," and Subsection 2.5S.4.7, "Response of Soil and Rock to Dynamic Loading." Revised Tables and Figures supporting these sections will be provided in a supplement to this RAI.	August 9, 2009